

#DOL

Copy 1
RM L5

TECH LIBRARY KAFB, NM

0144713

MAY 18 1958
14309
14632

NACA RM L58B18

7833

5877-86
TECHNICAL REPORT
AFL 2291

NACA

RESEARCH MEMORANDUM

HEAT TRANSFER FOR MACH NUMBERS UP
TO 2.2 AND PRESSURE DISTRIBUTIONS FOR MACH NUMBERS UP
TO 4.7 FROM FLIGHT INVESTIGATIONS OF A FLAT-PLATE
AND A HEMISPHERE-CONE

By Katherine C. Speegle, Leo T. Chauvin,
and Jack C. Heberlig

Langley Aeronautical Laboratory
Langley Field, Va.

UAC
BY AUTHORITY OF NASA TECH. PUB. (OFFICER AUTHORIZED TO CHANGE)
By ANNOUNCEMENT MR. #14632 June 1961
UAC

DATE OF REVIEW (MONTH)

7. July 1961
DATE

NATIONAL ADVISORY COMMITTEE
FOR AERONAUTICS

WASHINGTON

May 8, 1958



0144713

NATIONAL ADVISORY COMMITTEE FOR AERONAUTICS

RESEARCH MEMORANDUM

HEAT TRANSFER FOR MACH NUMBERS UP
TO 2.2 AND PRESSURE DISTRIBUTIONS FOR MACH NUMBERS UP
TO 4.7 FROM FLIGHT INVESTIGATIONS OF A FLAT-FACE-CONE
AND A HEMISPHERE-CONE

By Katherine C. Speegle, Leo T. Chauvin,
and Jack C. Heberlig

SUMMARY

Two blunt-nose models, a flat-face-cone and a hemisphere-cone, have been flight tested for Mach numbers up to 4.7. The flat face had a radius of 5 inches and the hemisphere had a radius of 6.5 inches. The conical sections had 14.5° half-angles. Heating data are presented for Mach numbers up to 2.2 and pressure data are presented for Mach numbers up to 4.6 for the flat-face-cone and up to 4.7 for the hemisphere-cone. Measured stagnation heating rates were lower than theoretical stagnation heating rates for both configurations. The measured laminar heating rates on the flat face were lower than those predicted by theory whereas the measured and theoretical laminar heating rates on the hemisphere were in good agreement. On both models transition occurred just ahead of the corner or hemisphere-cone juncture at a Mach number of 2. The transition Reynolds numbers based on momentum thickness were between 320 and 400 on the flat face and between 840 and 1,140 on the hemisphere. The turbulent heating rates along the conical sides of the flat-face model were much lower than those for the conical sides of the hemisphere-nose model.

Measured pressures at the corner and along the sides of the flat-face-cone were lower than those predicted by modified Newtonian theory. Measured pressures around the hemisphere-cone juncture were somewhat lower than those predicted by the Newtonian theory; however, the pressures measured along the conical sides of the hemisphere-cone were in very good agreement with the modified Newtonian theory.

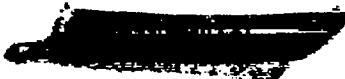
INTRODUCTION

The aerodynamic-heating characteristics of blunt noses are of basic importance in the design of long-range ballistic missiles. The Langley Pilotless Aircraft Research Division is conducting investigations to determine the heating characteristics for various blunt noses. (See refs. 1, 2, and 3.) Presented herein are the results of flight tests made at the Langley Pilotless Aircraft Research Station at Wallops Island, Va., for two noses: a truncated cone having a half-angle of 14.5° and nose-to-base radius ratio of about 0.6 where the base diameter is 17.6 inches, and a hemisphere-cone (half-angle of 14.5°) having a nose-to-base radius ratio of about 0.7 where the base diameter is also 17.6 inches. Basic flight data and heat-transfer data for the hemisphere-cone have already been published for Mach numbers from 2.32 to 3.14 in reference 4. The lower Mach number data not given in reference 4 were reduced and are presented herein in order that a more realistic comparison could be made with the data of the truncated cone.

Heat-transfer data for both models are presented for Mach numbers up to 2.2 and free-stream Reynolds number based on a length of 1 foot up to 14.5×10^6 whereas the pressure data for both models are presented for Mach numbers up to approximately 4.7.

SYMBOLS

C_p	pressure coefficient, $\frac{p_l - p_\infty}{0.7 p_\infty M_\infty^2}$
c_f	local skin-friction coefficient
c_p	specific heat, Btu/lb- $^\circ R$
h	altitude, ft
M	Mach number
N_{St}	Stanton number
P_1, P_2, \dots, P_6	pressure stations (see figs. 2(a) and 3(a))
p	pressure, lb/sq in. abs



q	heating rate, Btu/sq ft-sec
R	Reynolds number
r	nose radius, in.
T_1, T_2, \dots, T_{18}	thermocouple stations (see figs. 2(a) and 3(a))
T	temperature, $^{\circ}R$
t	time, sec
x	surface distance from stagnation point, in.
ρ	density of air, slugs/cu ft
ρ_w	density of wall material, lb/cu ft
τ	thickness, ft
ϕ	meridian angle, deg

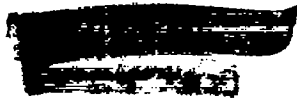
Subscripts:

l	outside boundary layer
t	stagnation
w	pertaining to wall
∞	free stream
1	based on a length of 1 foot
2	behind normal shock

MODELS

Model A, Flat-Face-Cone

The general configuration of the flat-face-cone model (model A) is shown in figure 1 on the launcher. This test nose was mounted on the forward end of a standard Nike booster rocket motor, designated JATO, 2.5-DS-59000, X216A2, which is stabilized by four fins equally spaced



about the rearward end of the rocket motor. The first-stage booster was a standard Honest John rocket motor, designated JATO, 4-DS-105,000,M6.

The length of the nose was 14.25 inches. The flat face had a radius of 5 inches and the conical section had a base radius of 8.8 inches. The flat-face-cone juncture was rounded to a radius of 0.25 inch. A sketch of the nose section is shown in figure 2(a). The nose was constructed from Inconel approximately 0.031 inch thick. The exterior surface of the flat face was highly polished to a finish of 2 microinches (as measured by an interferometer) while the sides of the model were polished to a finish of 5 microinches. A closeup photograph of the nose is shown in figure 2(b). The measured thicknesses of the skin after polishing are presented in table I. For structural purpose the nose skin was backed with a layer of 3/8-inch balsa, mounted on a 3/8-inch magnesium structure which also served to shield the telemeter from thermoradiation.

Model B, Hemisphere-Cone

The booster and sustainer system of the hemisphere-cone model (model B) was identical to model A. In general, the construction details were the same as model A, with model B having a length of 15.72 inches. The hemisphere had a radius of 6.5 inches. The hemisphere-cone juncture occurred at a point 76° along the hemisphere from the stagnation point. A sketch of the nose section is presented in figure 3(a) and a photograph showing the high degree of polish is presented in figure 3(b). The hemispherical portion of the nose was polished to a roughness of 2 to 3 microinches and the conical portion to a roughness of 3 to 5 microinches as measured with an interferometer. More detailed construction information is presented in reference 4. Measured skin thicknesses after polishing are given in table II.

INSTRUMENTATION

Model A

An NACA 10-channel telemeter was carried in the forward portion of the model and transmitted wall temperatures, pressures, and accelerations. There were 18 temperature pickups. The 12 pickups on the conical section were commutated every 0.2 second and the 6 pickups on the face were commutated every 0.1 second. No. 30 chromel-alumel thermocouples were welded in rays to the inner surface of the skin at the stations shown in figure 2(a). Twelve thermocouples were located in one ray beginning at the stagnation point and continuing toward the base of the nose. Two rays containing three thermocouples each were located 75° and 255° from the first ray.

In order to reduce heat losses to the balsa backing, cutouts were made in the balsa in the region of each thermocouple on the flat face by drilling 1/2-inch-diameter holes and by making a groove 1.5 inches wide by 1/8 inch deep along each ray of thermocouples on the conical section.

The six pressure orifices were made by welding stainless-steel tubing (outer diameter, 0.09 inch; inner diameter, 0.06 inch) to the skin and were located along a ray 180° from the 12-thermocouple ray. The pressure cells read absolute pressures.

Model B

The instrumentation details for model B were similar to model A. There were 12 chromel-alumel thermocouples located as shown in figure 3(a). Temperatures were sampled for all thermocouples at about every 0.1 second. Six pressures were measured at locations shown in figure 3(a). The model also contained thrust and drag accelerometers.

General

Model velocities were obtained from CW Doppler radar. Atmospheric conditions were measured by means of radiosondes launched near the time of flight and tracked by a Rawin set AN/GMD-1A. Trajectory data were obtained by using an NACA modified SCR-584 position radar.

TESTS

The models were launched at an elevation angle of 55°. The Honest John booster accelerated the models to a Mach number of 2.2. Model A coasted for 0.7 second and was then accelerated to a Mach number of 4.6 by the Nike. Model B had a coast period of 1.7 seconds before the Nike fired and accelerated the model to a Mach number of 4.7. Time histories of free-stream Reynolds number based on a length of 1 foot, free-stream Mach number, and altitude for each model are shown in figure 4. Atmospheric conditions as obtained from the radiosonde measurements are presented in figure 5.

DATA REDUCTION

Temperature measurements for both models were reduced to heating rates by using the following relation

$$q = \frac{dT}{dt} \rho_w \tau_w c_{p,w}$$

The skin thickness τ_w was measured (tables I and II), the density of Inconel ρ_w was known, and the specific heat of Inconel $c_{p,w}$ as a function of temperature was obtained from reference 5. The rate of temperature change with time $\frac{dT}{dt}$ was found by mechanically differentiating the measured temperature-time curve.

Heating-Rate Theories

The theoretical heating rates for the stagnation point of both models were evaluated by the theory of Sibulkin (ref. 6). The stagnation-point theory was modified by using the measured pressure distribution at a Mach number of 2 as presented in reference 7 for the flat face. For the hemisphere, Sibulkin theory was used along with the velocity distribution of Roshotko and Cohen (ref. 8).

The theory for the laminar heat-transfer distribution along the hemisphere was taken from reference 9. The theory for the laminar heat-transfer distribution across the flat face was determined by the theory of Stine and Wanlass (ref. 10) in conjunction with the pressure distribution from reference 7. This theory is presented for only 70 percent of the flat face since the evaluation of the pressure-gradient parameter for this theory becomes inaccurate as the corner of the flat face is approached. Lees' blunt-nose theory (ref. 9) was used for the flat face also. The measured pressure distribution across the face as shown in reference 7 and the measured pressures along the 0.25-inch radius of the corner as presented in this report were faired and used to get the velocity distribution for this specific blunt-nose shape.

The theory presented for the sides of both models is Van Driest's conical theory (ref. 11) with the assumption that the length used in the Reynolds number is the surface length from the stagnation point and that $N_{St} = 0.5c_f$.

~~CONFIDENTIAL~~

Local Conditions

The local conditions for model A were calculated by using the experimental flat-face pressure distribution for $M_\infty = 2$ of reference 7. The six measured pressures were used to calculate local conditions from the flat-face-cone juncture back along the side of the nose. The most rearward pressure measurement was assumed constant for the remaining conical section.

The local conditions for model B were calculated for the hemisphere by using modified Newtonian theory (ref. 12). The pressures over the conical portion of the nose were measured and used for obtaining local conditions.


RESULTS AND DISCUSSION

Pressure Measurements

Model A. - Pressures were measured near the corner and on the sides of model A at the locations shown in figure 2(a). The ratios of the measured local pressure to the total pressure behind the normal shock are shown for several Mach numbers in figure 6(a) along with the measured pressure ratios for the flat faces of references 7 and 13. For the flat-face portion of the nose the theoretical pressure distribution of Maccoll and Codd for Mach number of 1.5 (ref. 14) is presented. The data obtained from the measurements on the two flat faces are in good agreement with the Maccoll and Codd theory and substantiate its use later in this report to obtain heat-transfer theory on the flat face. Results obtained with the use of the modified Newtonian theory for Mach numbers of 1.5 and 4.55 (ref. 12) along the conical side of the nose are also shown. The measurements on the 0.25-inch radius of the flat-face cone are much lower than theory and are possibly due to separation or overexpansion. After the corner the pressures only tend to approach those predicted by the Newtonian theory for a blunt-nose cone for the lower Mach numbers but reach those predicted by the theory for the highest reported Mach number, which is 4.55. This is a normal trend since overexpansion decreases with increasing Mach number.

Figure 6(b) also shows the measured pressures in the form of pressure coefficients along with the measurements of reference 13 and the theory of reference 12 (Newtonian blunt-nose theory). The coefficients show a rather large Mach number effect and possibly a Reynolds number effect around the corner. Again it may be noted that the overexpansion is larger for the lower Mach numbers. The experimental data only tend to approach Newtonian theory, with the least-expanded higher Mach number

~~CONFIDENTIAL~~



data along the conical sides showing the best agreement - the lower the Mach number, the progressively poorer the agreement.

Model B.- Pressures were also measured on model B for station locations on the hemisphere and on the conical sides as shown in figure 3(a). The ratios of the measured local pressure to the total pressure behind the normal shock are given for several Mach numbers in figure 7(a) along with Newtonian theory for the entire blunt shape. The data are in good agreement with theory except in the region around the hemispherical-cone juncture where the pressures are reduced probably from overexpansion. The data are in very good agreement with theory on the conical sides.

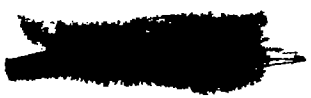
The measured pressures are presented for model B as pressure coefficients in figure 7(b). The good agreement with Newtonian theory is again noted except in the vicinity of the hemisphere-cone juncture. The lower Mach number data show a strong overexpansion with the expansion decreasing with increasing Mach number. For a Mach number of 4.7, the expansion is barely detected. The Reynolds number along with Mach number may also have some effect.

General.- The measured pressures on both model A and model B indicate an overexpansion near the junctures of the faces and sides of the noses. The expansion is much greater for the flat-face-cone with the pressures remaining lower than those obtained by using the Newtonian theory along the conical sides. The pressures along the conical sides of the hemisphere-cone model are in very good agreement after the slight overexpansion at the juncture.

Heat Transfer

Model A.- The faired temperature-time curve for each measuring station is shown for model A in figure 8. Temperature channel telemetering failed at sustainer firing; therefore, temperatures are presented for only 0 to 5.6 seconds of the flight. The temperature distributions across the face and along the side of the nose are shown for several times and Mach numbers in figure 9. Transition is indicated by the sudden rise in temperature between the 70- and 95-percent flat-face stations. The temperatures in the region around the corner stay low for the entire measuring period with the station just after the corner $x/r = 1.2$ having a maximum temperature rise of about 30° , less than one-half the laminar temperature rise of the face.

The measured heating rates are presented for the 18 temperature stations as a variation with time in figure 10. The stagnation point heating rates predicted by the Sibulkin theory, modified for a flat face, are shown in figure 10(a) along with the measured heating rate.



At the point of maximum measured heating rate the measured rate is only 85 percent of the predicted rate. For earlier flight times, the measured rate is less than 85 percent of theory. However, data are less reliable at these earlier times because of the low rates being measured. Previous tests (ref. 15) on a blunt-nose model have also shown rates of around 85 percent of that predicted by theory. Since the reference model was not backed with balsa, it is felt that this disagreement with theory is probably not an indication of heat loss to the backing material. Heating rates for three points around the conical section of the nose - all the same distance from the stagnation point - are shown in the top plot of figure 10(d) for comparison. The heating rates for station 18 are as much as 20 percent lower than those for station 12 but both are still of a turbulent level as will be noted later.

Figure 11 shows the ratio of the measured heating rate across the flat face to the theoretical stagnation heating rate for several Mach numbers, along with the theoretical laminar distributions of Stine and Wanlass and of Lees, based on the pressure data of reference 7. The measurements fall far below theory for all Mach numbers up to the 50-percent station. Transition apparently is starting between the 70- and 95-percent stations. Even though the measurements on the corner generally fall lower than the laminar measurements on the flat face, they are higher than laminar theory and indicate turbulence.

The ratio of measured heating rate on the flat face to the measured stagnation heating rate is shown in figure 12. The theories of Stine and Wanlass and of Lees are also shown. The percentage variation of the heating rate across the face agrees well with the laminar theory until transition begins between the 70-percent and 95-percent stations. The 95-percent-station measurements are somewhat higher than theory and indicate transition.

Distributions of the heating rates for the entire flat-face-cone nose are shown in figure 13 for four different flight times; also shown are the distributions of local Reynolds number, local Mach number, and ratio of wall temperature to local static temperature. The flat-face portion of the data is presented again in this figure only to show the comparison of heating rates on the sides with those on the flat face. The expansion occurring at the flat-face-cone juncture results in heating rates of a laminar level after transitional flow existed at the last station, $R_7 = 4.5 \times 10^6$ on the flat face. The data indicate that the heating remains at the laminar level for approximately 1 inch after the corner. The measured heating rates in the region around the corner for the test Mach numbers between 1.5 and 2.2 are in good agreement with the Lees blunt-nose theory extended past the corner. The data are also approximately on the same level as those predicted by the Van Driest conical laminar theory. In the absence of a simple method for predicting

heating in the low-pressure region at the corner, the Van Driest theory appears to be adequate. The measured turbulent heating rates along the conical surface of the nose agree well with the rates predicted by the Van Driest conical turbulent theory by assuming the pressures measured for temperature station 10 exist along the rear portion of the cone. The results predicted by the Van Driest conical turbulent theory is also presented for the case in which the modified Newtonian pressure distribution is assumed. The measured heating rate is shown to be lower than that which might be estimated by using this theoretical pressure distribution.

Model B.—Faired curves for skin-temperature measurements for the early part of the flight for model B are presented in figure 14 as a function of time. Cross plots of the temperature are presented in figure 15 as a function of x/r for several times and Mach numbers. At 4.7 seconds and later, transition is indicated for station 9 ($x/r = 1.33$), the tangent point of the hemisphere-cone, by the sudden rise in temperature.

The measured heating rates are given in figure 16 as a function of time for all temperature measuring stations. The maximum measured stagnation heating rate is 87.5 percent of the hemispherical stagnation-point heating rate as given by Sibulkin.

The measured heating rates for the hemisphere are given in figure 17 as a ratio of measured heating rate to theoretical heating rate at the stagnation point (ref. 6) as a function of x/r for various Mach numbers. The figure shows that transition begins between station 7 ($x/r = 0.78$) and station 8 ($x/r = 1.05$) for $M_\infty = 2.0$ and 2.2 . The Reynolds number based on momentum thickness, as computed from reference 16, at station 8 is approximately 1,150. Experiment and theory are in rather good agreement for the forward portion of the hemisphere.

Experimental heating rates around the hemisphere as a percent of experimental stagnation heating rates are shown in figure 18. The percentage variation is again in very good agreement with theory, and transition is again shown to occur between station 7 and station 8 for $M_\infty = 2.0$ and 2.2 .

Distributions of the heating rates for the entire nose section of the hemisphere-cone are shown in figure 19 for several Mach numbers; also shown are the distributions of local Reynolds number, local Mach number, and ratio of wall temperature to local static temperature. For $M_\infty = 1.5$, transition possibly occurs between $x/r = 1.64$ and 2.10 (R_1 between 8.5 and 11.5×10^6). This is between 2 and 5 inches behind the hemisphere-cone juncture and is shown in figure 19(a). This indication

of transition may be due to a stray point in the data inasmuch as the last station on the cone ($x/r = 2.82$) appears to be laminar. Figure 19(b) shows transition at the most rearward station on the cone ($R_L = 17.2 \times 10^6$) and this station is 9.72 inches from the point of tangency for the hemisphere-cone.

As has been stated previously, transition occurs on the hemisphere for x/r between 0.78 and 1.05 (R_L between 6.0 and 6.5×10^6) for $M_\infty = 2.0$ and 2.2 as shown in figures 19(c) and 19(d). For $M_\infty = 2.0$, the heating rate does not reach a fully turbulent level until $x/r = 2.82$. The heating rate reaches the turbulent level for $M_\infty = 2.2$ at $x/r = 1.33$, which is the hemisphere-cone tangent point. Results obtained with the Van Driest conical laminar and turbulent theories by using measured pressure distributions give accurate predictions for the heating rates along the conical portion of the hemisphere-cone. Modified Newtonian pressure distributions are in excellent agreement with the measured pressures in predicting heating rates on the conical sides.

General. - The ratios of heating rate to hemisphere stagnation theory heating rate are presented in figure 20 for both flat-face-cone and the hemisphere-cone noses at $M_\infty = 2.2$. Transition occurred for both models at $x/r \approx 0.9$. The Reynolds number of transition based on momentum thickness on the flat face was between 320 and 400. For the hemisphere it was between 840 and 1,140. The laminar heating rate before transition on the flat face was 40 to 50 percent lower than the hemisphere heating rate. However, the area of laminar heating on the flat face is between 0.29 and 0.40 square foot and on the hemisphere between 0.46 and 0.62 square foot, the area of laminar heating on the flat face being only 60 to 80 percent of the area on the hemisphere. The maximum heating rate along the conical sides of the hemisphere-cone was about 100 percent greater than the heating rate on the conical sides of the flat-face-cone.

CONCLUDING REMARKS

Flight tests have been made on two blunt-nose shapes, one a flat face and the other a hemisphere, both having 14.5° half-angle conical sides. Boundary-layer transition occurred on the flat face just before the corner for Mach numbers of 1.5 and 2.2. Transition occurred on the conical sides of the hemisphere model for Mach numbers from 1.5 to 1.8 and on the hemisphere just before the hemisphere-cone juncture for Mach numbers from 2.0 to 2.2. The laminar heating rate on the flat face was approximately 40 to 50 percent lower than on the hemisphere. However, the area of laminar heating on the flat face is between 0.29 and 0.40

square foot and on the hemisphere between 0.46 and 0.62 square foot, the area of laminar heating on the flat face being only 60 to 80 percent of the area on the hemisphere. The maximum turbulent heating rate along the conical sides of the hemisphere-cone was about 100 percent greater than the maximum turbulent heating rate on the conical sides of the flat-face-cone.

The measured pressures at the corner and along the sides of the flat-face-cone are lower than those predicted by modified Newtonian theory. Measured pressures around the hemisphere-cone juncture are also somewhat lower than those predicted by the Newtonian theory; however, the measured pressures along the conical sides of the hemisphere-cone model are in very good agreement with modified Newtonian theory.

Langley Aeronautical Laboratory,
National Advisory Committee for Aeronautics,
Langley Field, Va., February 4, 1958.

REFERENCES

1. Chauvin, Leo T.: Aerodynamic Heating of Aircraft Components. NACA RM L55L19b, 1956.
2. Rumsey, Charles B., and Lee, Dorothy B.: Heat-Transfer Measurements in Free Flight at Mach Numbers Up to 14.6 on a Flat-Faced Conical Nose With a Total Angle of 29° . NACA RM L57L03, 1958.
3. Bland, William M., Jr., Swanson, Andrew G., and Kolenkiewicz, Ronald: Free-Flight Aerodynamic Heating Data at Mach Numbers Up to 10.9 on a Flat-Faced Cylinder. NACA RM L57K29, 1958.
4. Buglia, James J.: Heat Transfer and Boundary-Layer Transition on a Highly Polished Hemisphere-Cone in Free Flight at Mach Numbers Up to 3.14 and Reynolds Numbers Up to 24×10^6 . NACA RM L57D05, 1957.
5. Ginnings, Defoe C., and Thomas, Eugenia: The Electrical Resistance and Total Radiant Emittance of Inconel in the Range 0° to $1,000^\circ$ C. NBS Rep. 4111 (NACA Contract S54-52), Nat. Bur. Standards, May 1955.
6. Sibulkin, M.: Heat Transfer Near the Forward Stagnation Point of a Body of Revolution. Jour. Aero. Sci. (Readers' Forum), vol. 19, no. 8, Aug. 1952, pp. 570-571.
7. Stoney, William E., Jr., and Swanson, Andrew G.: Heat Transfer Measured on a Flat-Face Cylinder in Free Flight at Mach Numbers Up to 13.9. NACA RM L57E13, 1957.
8. Reshotko, Eli, and Cohen, Clarence B.: Heat Transfer at the Forward Stagnation Point of Blunt Bodies. NACA TN 3513, 1955.
9. Lees, Lester: Laminar Heat Transfer Over Blunt-Nosed Bodies at Hypersonic Flight Speeds. Jet Propulsion, vol. 26, no. 4, Apr. 1956, pp. 259-269.
10. Stine, Howard A., and Wanlass, Kent: Theoretical and Experimental Investigation of Aerodynamic-Heating and Isothermal Heat-Transfer Parameters on a Hemispherical Nose With Laminar Boundary Layer at Supersonic Mach Numbers. NACA TN 3344, 1954.
11. Van Driest, E. R.: The Problem of Aerodynamic Heating. Aero. Eng. Rev., vol. 15, no. 10, Oct. 1956, pp. 26-41.

12. Oliver, Robert E.: An Experimental Investigation of Flow Over Simple Blunt Bodies at a Nominal Mach Number of 5.8. GALCIT Memo. No. 26 (Contract No. DA-04-495-Ord-19), June 1, 1955.
13. Carter, Howard S., and Bressette, Walter E.: Heat Transfer and Pressure Distribution on Six Blunt Noses at a Mach Number of 2. NACA RM L57C18, 1957.
14. Maccoll, J. W., and Codd, J.: Theoretical Investigation of the Flow Around Various Bodies in the Sonic Region of Velocities. British Theoretical Res. Rep. No. 17/45, B.A.R.C. 45/19, Ministry of Supply, Armament Res. Dept., 1945.
15. Garland, Benjamin J., and Chauvin, Leo T.: Measurements of Heat Transfer and Boundary-Layer Transition on an 8-Inch-Diameter Hemisphere-Cylinder in Free Flight for a Mach Number Range of 2.00 to 3.88. NACA RM L57D04a, 1957.
16. Bromberg, Robert: A Note on the Calculation of Momentum Thickness Reynolds Number in a Boundary Layer With Pressure Gradient. Rep. No. GM-TN-21, The Ramo-Wooldridge Corp., Guided Missile Res. Div., May 11, 1956.

TABLE I

STATION LOCATION AND SKIN THICKNESS
FOR MODEL A

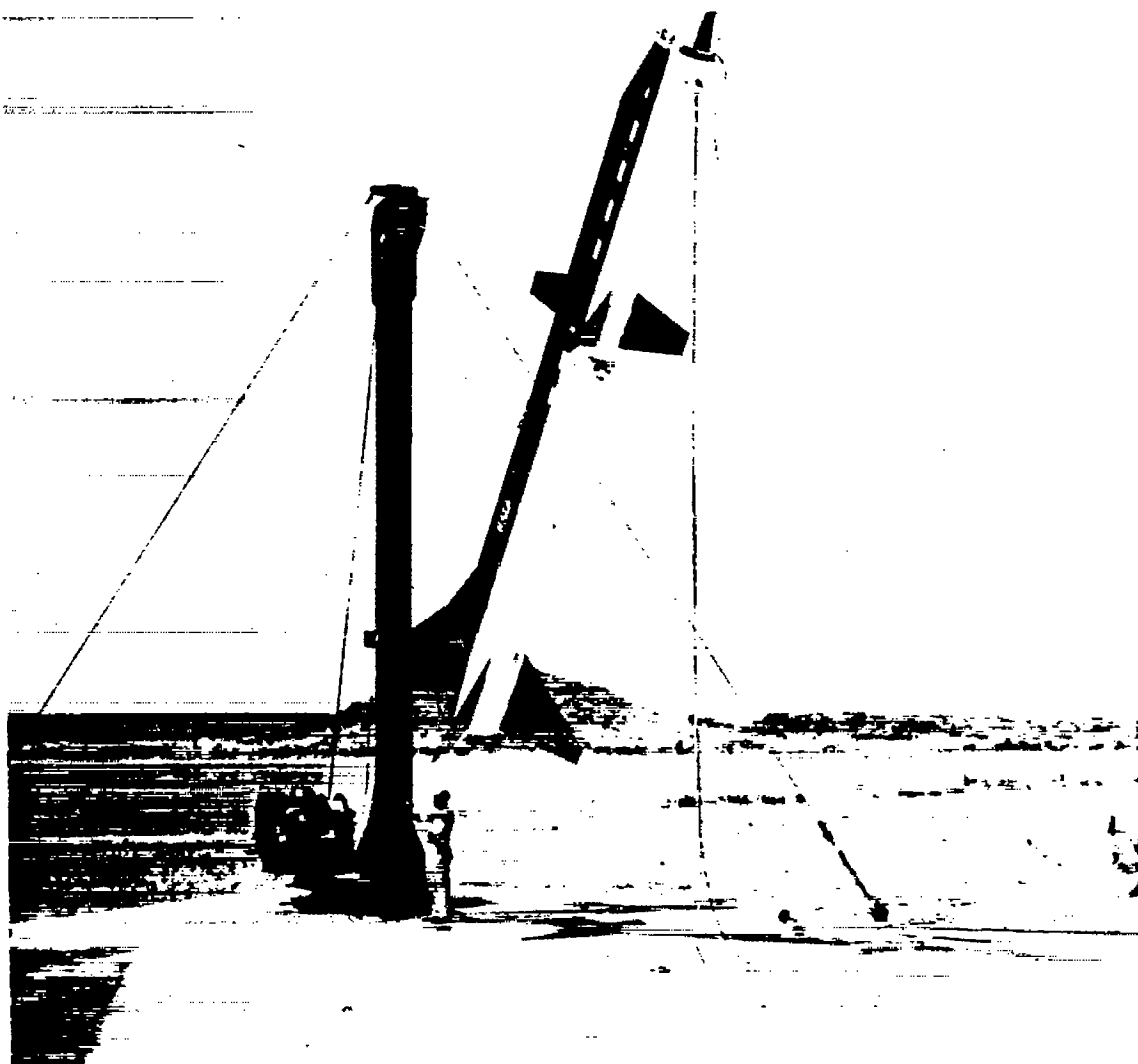
Station (see fig. 2(a))	x/r	Skin thickness, in.
T ₁	0	0.029
T ₂	.3	.027
T ₃	.5	.028
T ₄	.7	.030
T ₅	.95	.025
T ₆	.97	.022
T ₇	1.10	.021
T ₈	1.20	.020
T ₉	1.50	.023
T ₁₀	2.00	.026
T ₁₁	2.70	.025
T ₁₂	3.60	.027
T ₁₃	1.60	.027
T ₁₄	2.40	.027
T ₁₅	3.60	.028
T ₁₆	1.60	.024
T ₁₇	2.40	.026
T ₁₈	3.60	.028
P ₁	0.95	
P ₂	.97	
P ₃	1.10	
P ₄	1.20	
P ₅	1.50	
P ₆	2.00	

TABLE II

STATION LOCATION AND SKIN THICKNESS

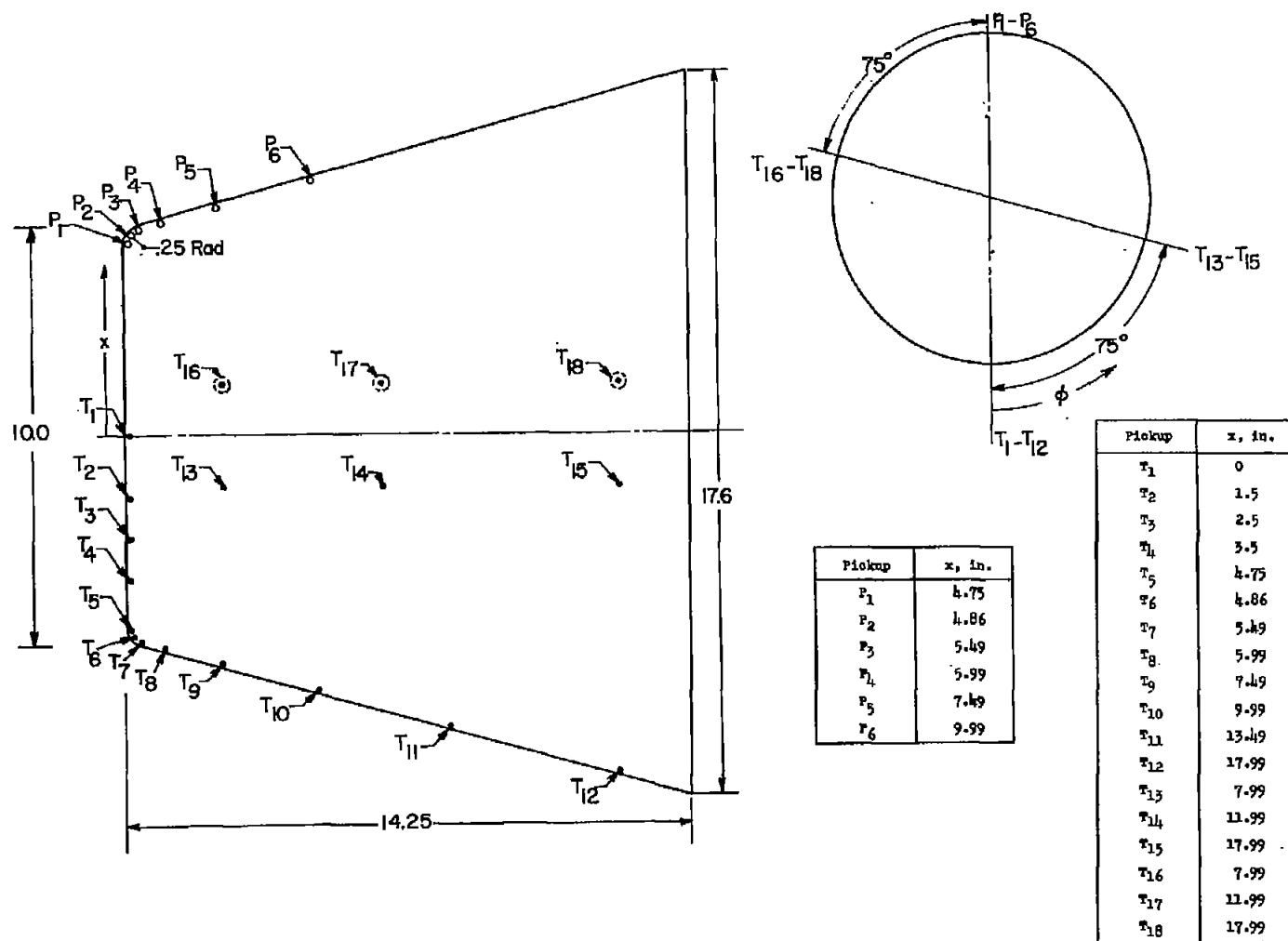
FOR MODEL B

Station (see fig. 3(a))	x/r	Skin thickness, in.
T ₁	0	0.024
T ₂	.17	.025
T ₃	.30	.026
T ₄	.42	.025
T ₅	.54	.025
T ₆	.66	.023
T ₇	.78	.024
T ₈	1.05	.027
T ₉	1.33	.028
T ₁₀	1.64	.031
T ₁₁	2.10	.030
T ₁₂	2.82	.030
P ₁	0.96	
P ₂	1.13	
P ₃	1.33	
P ₄	1.50	
P ₅	1.67	
P ₆	2.74	



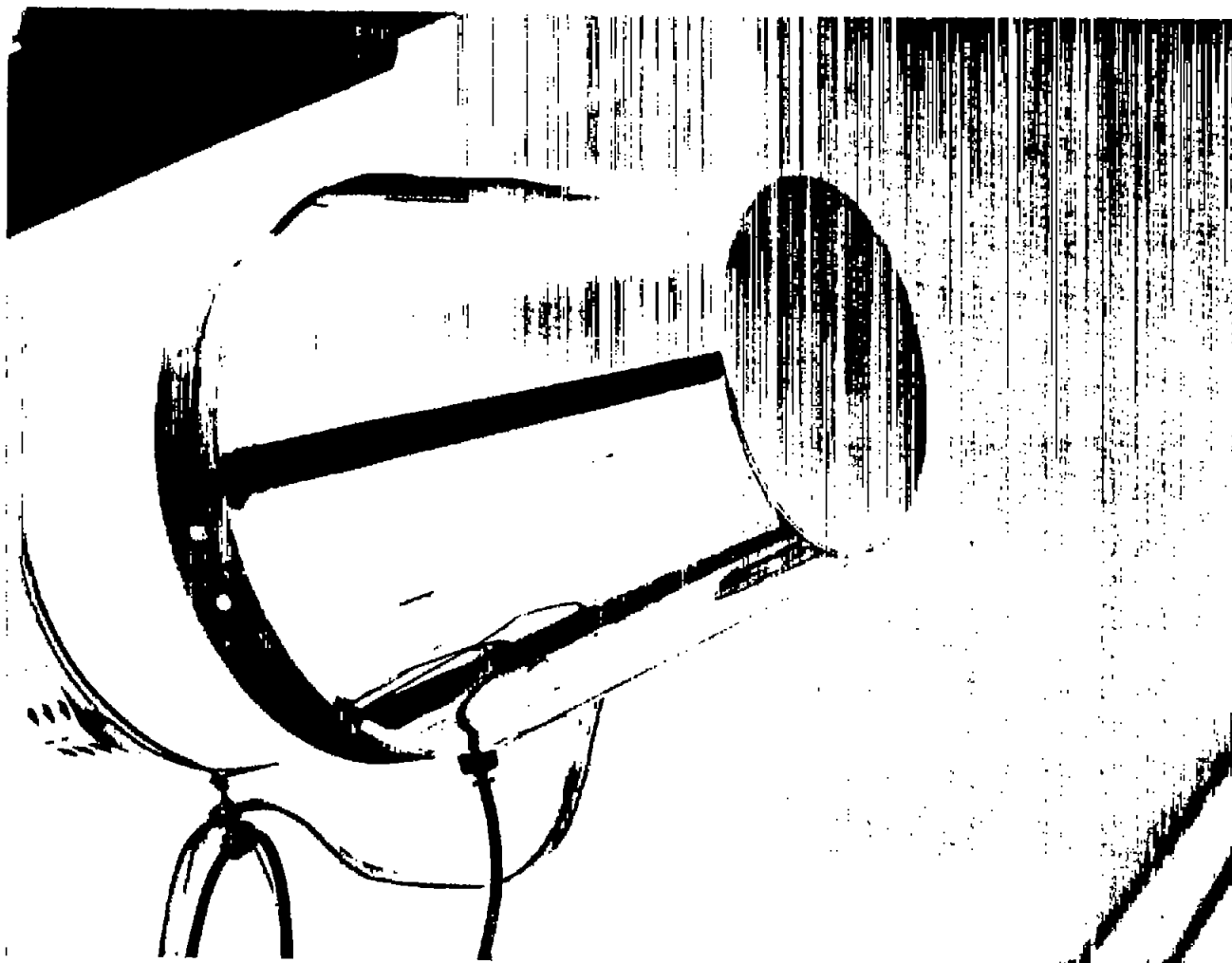
L-57-3250

Figure 1.- Photograph of the flat-face configuration, model A, on the launcher.



(a) Sketch of the nose. (All dimensions are in inches unless otherwise noted.)

Figure 2.- Flat-face configuration, model A.

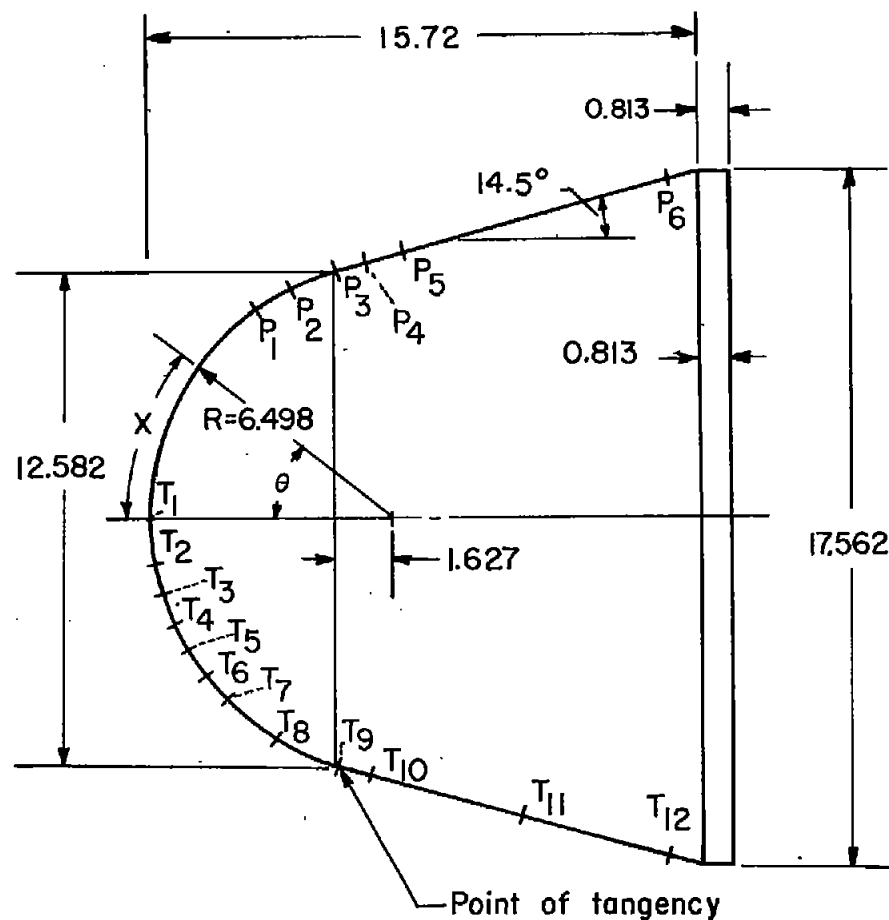


(b) Photograph of the nose.

L-57-3252

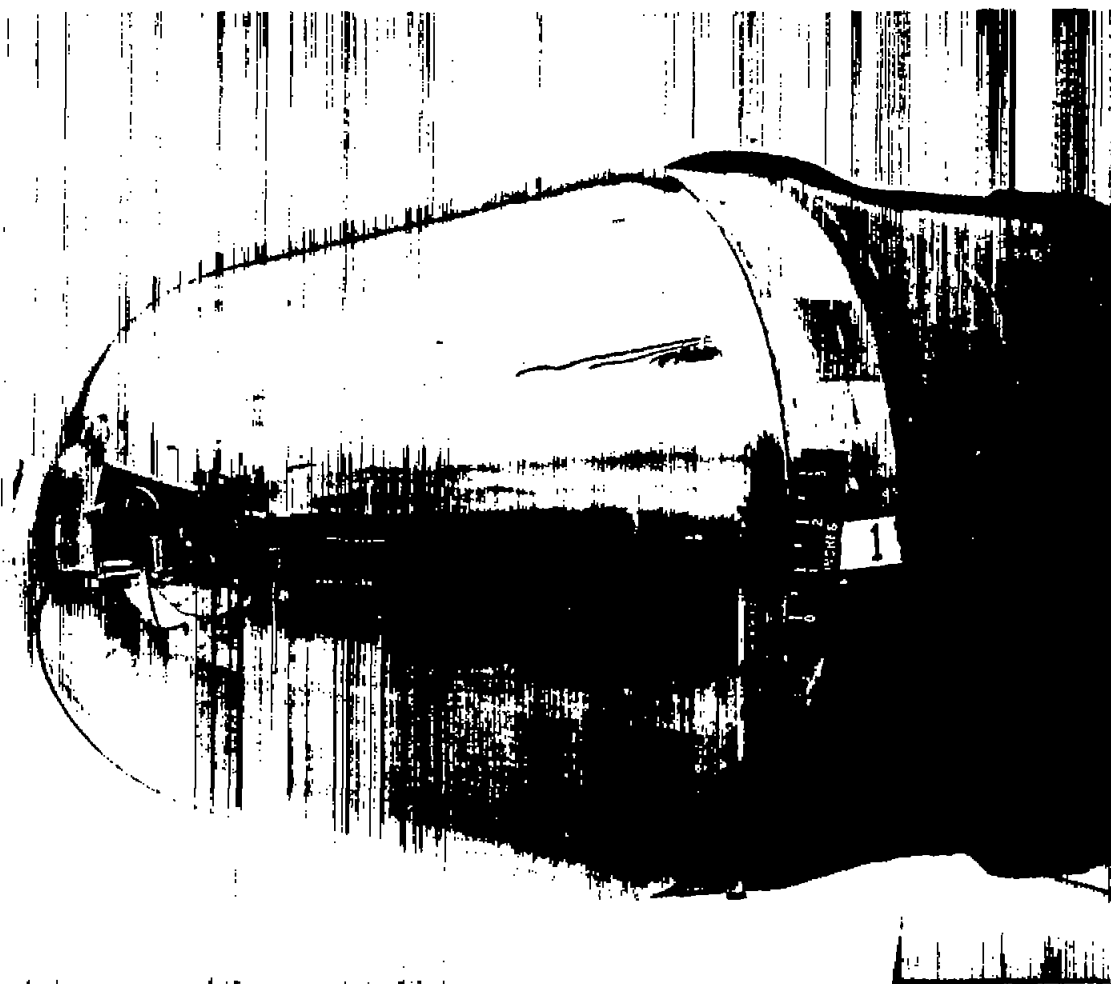
Figure 2.- Concluded.

Pickup	θ , deg	x , in.
P ₁	55	6.23
P ₂	65	7.37
P ₃	76	8.62
P ₄		9.72
P ₅		10.84
P ₆		17.81
T ₁	0	0
T ₂	10	1.13
T ₃	17	1.93
T ₄	24	2.72
T ₅	31	3.52
T ₆	38	4.31
T ₇	45	5.10
T ₈	60	6.81
T ₉	76	8.62
T ₁₀		10.64
T ₁₁		13.64
T ₁₂		18.34



(a) Sketch of the nose. (All dimensions are in inches unless otherwise noted.)

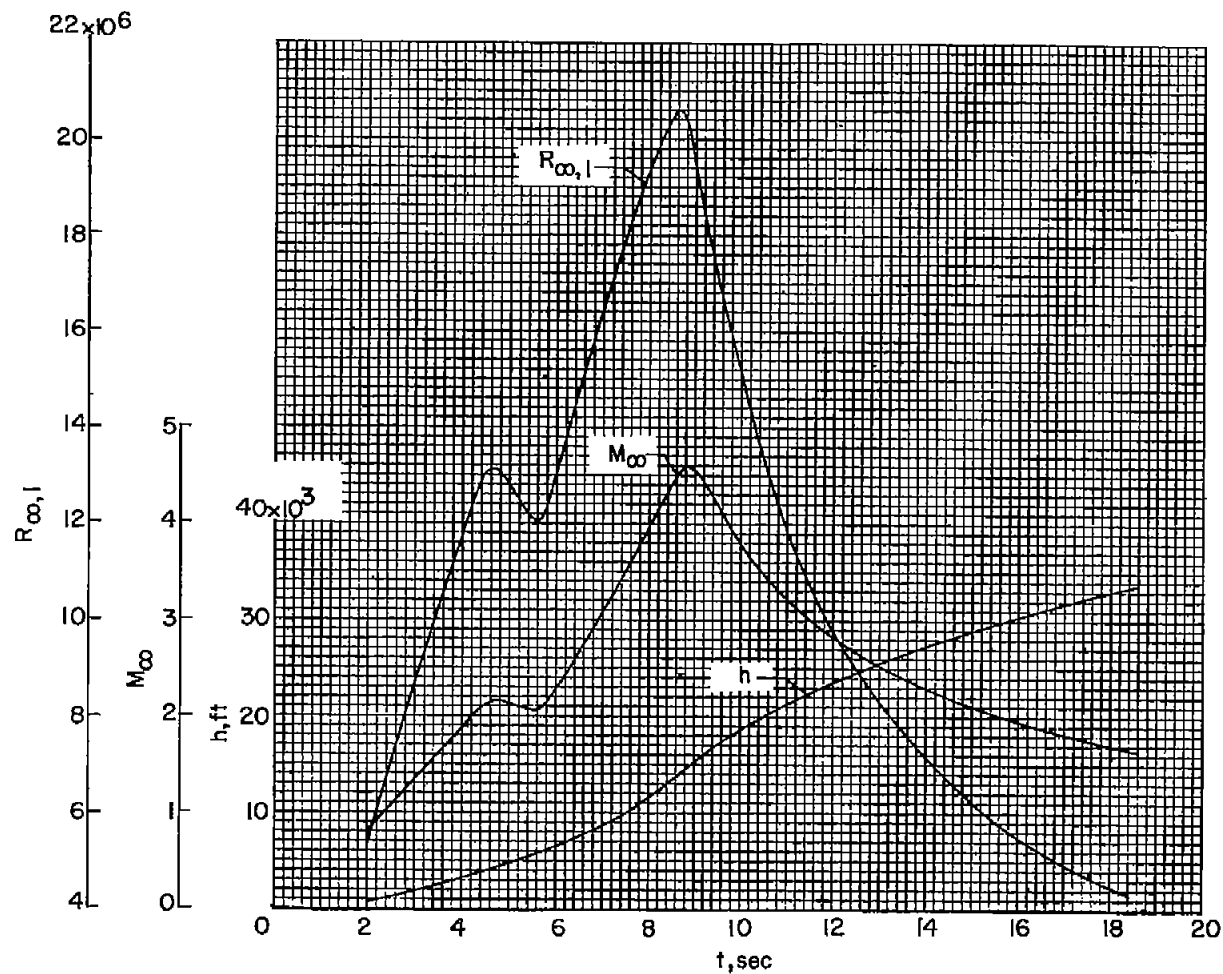
Figure 3.- Hemisphere configuration, model B.



(b) Photograph of the nose.

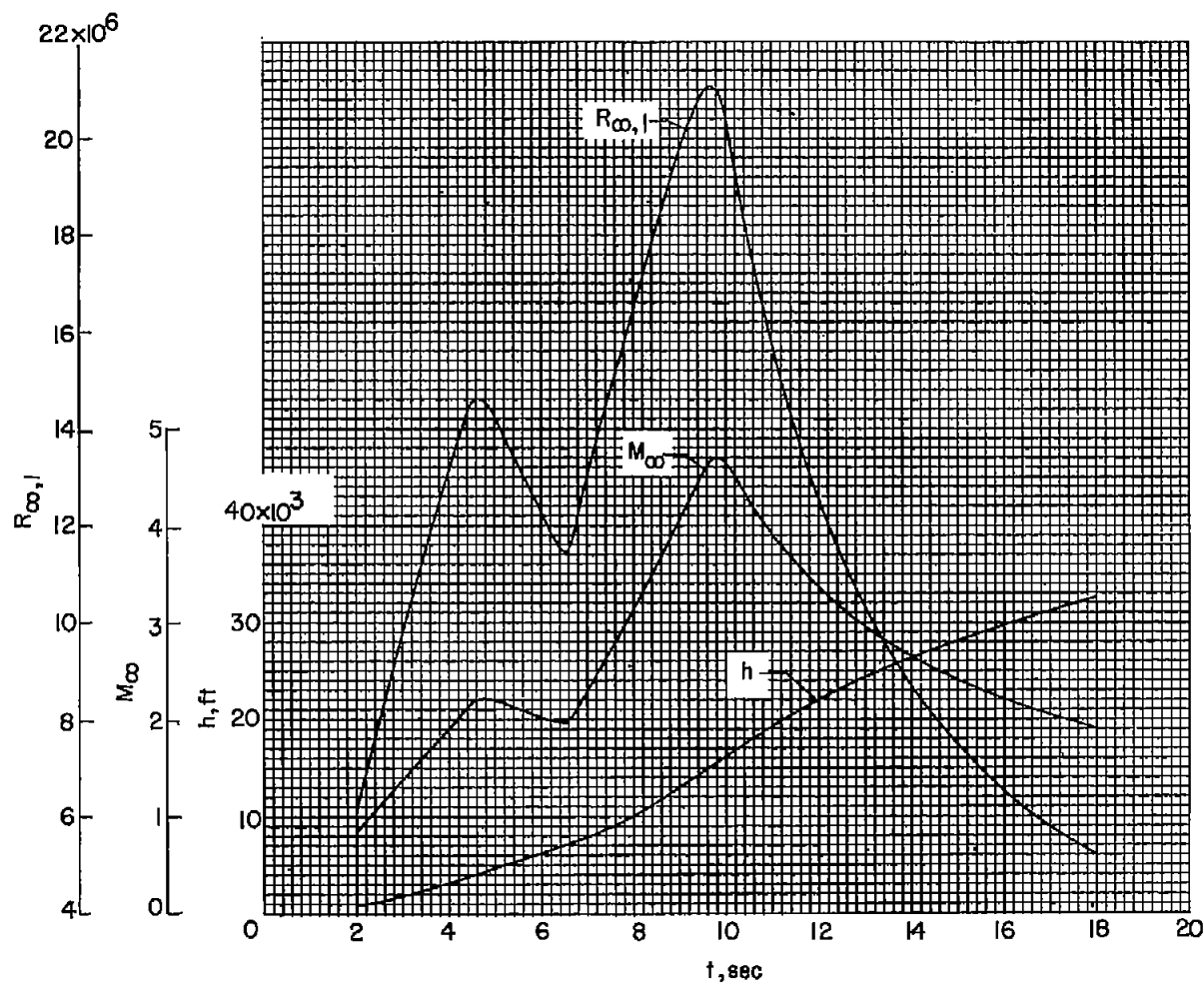
L-96346

Figure 3.- Concluded.



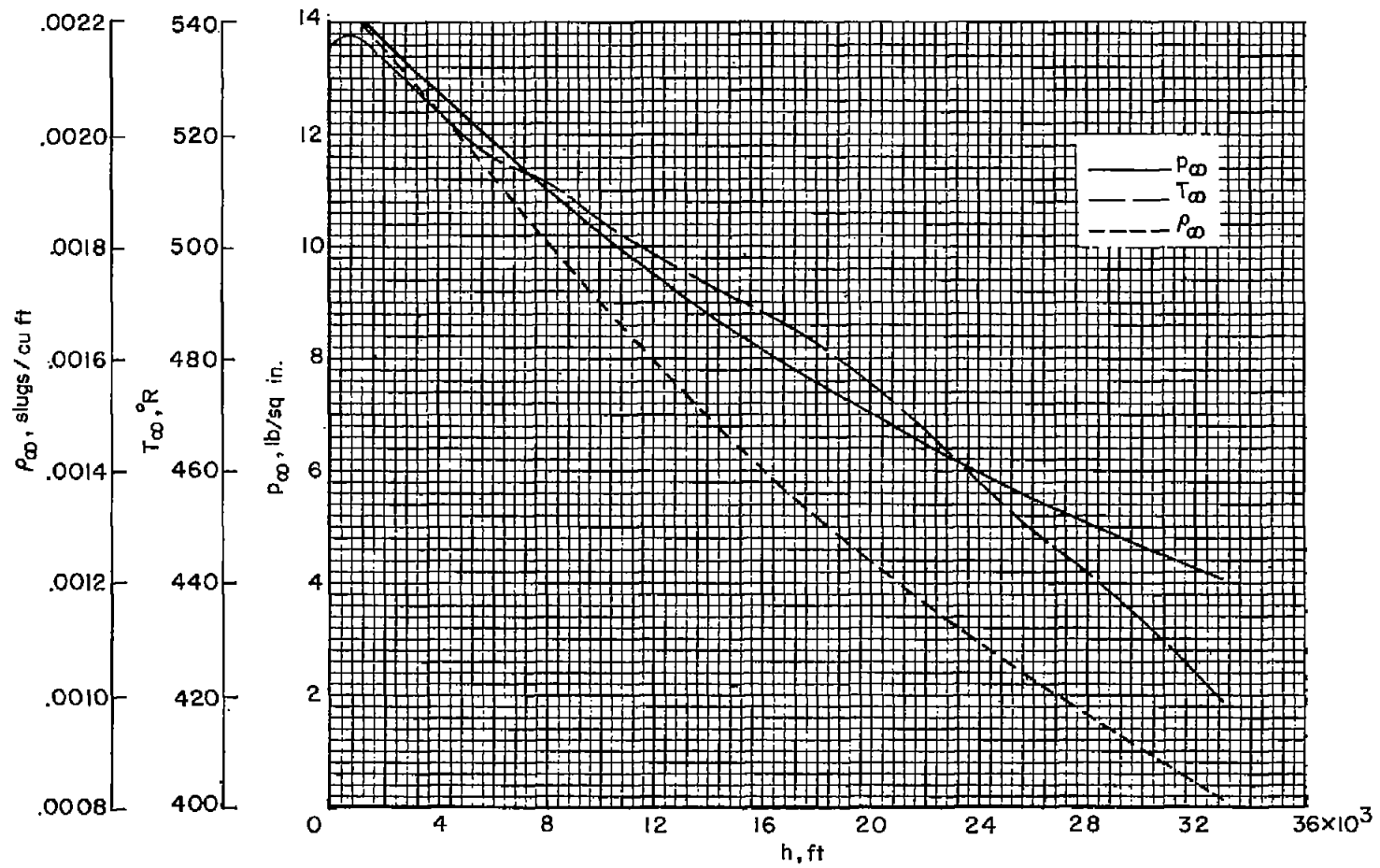
(a) Model A.

Figure 4.- Time histories of free-stream Reynolds number based on a length of 1 foot, free-stream Mach number, and altitude.



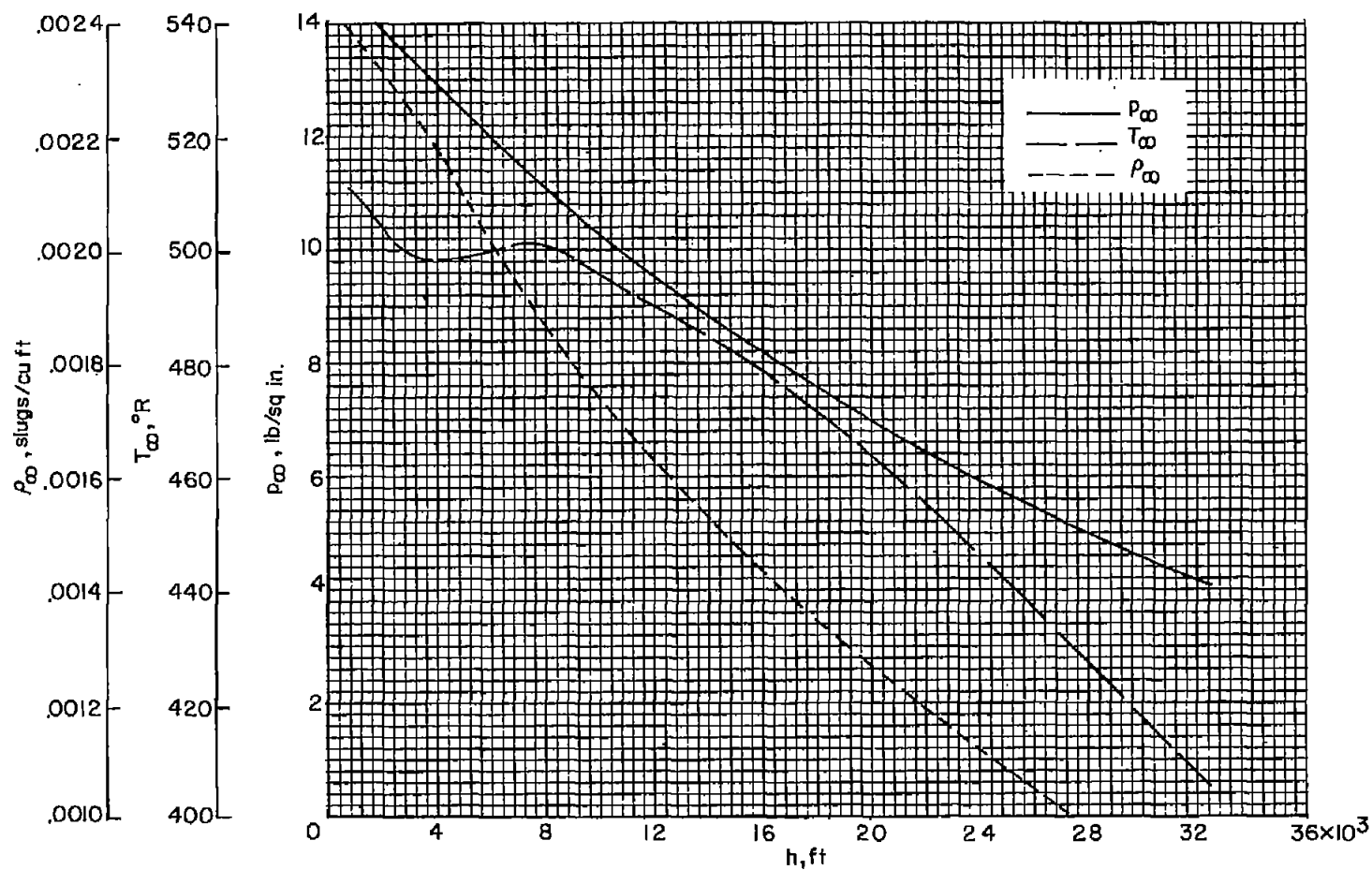
(b) Model B.

Figure 4.- Concluded.



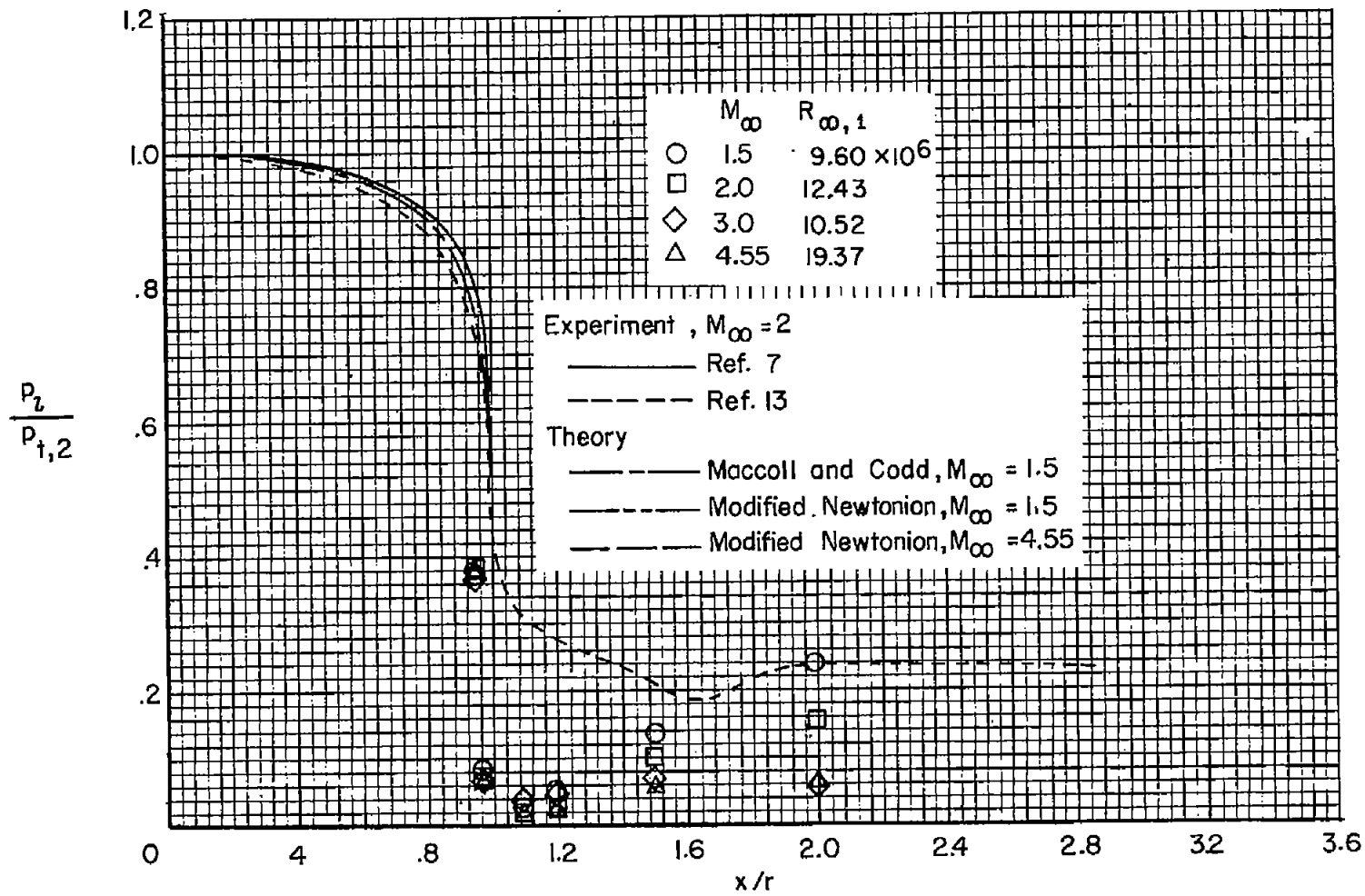
(a) Model A.

Figure 5.- Atmospheric conditions.



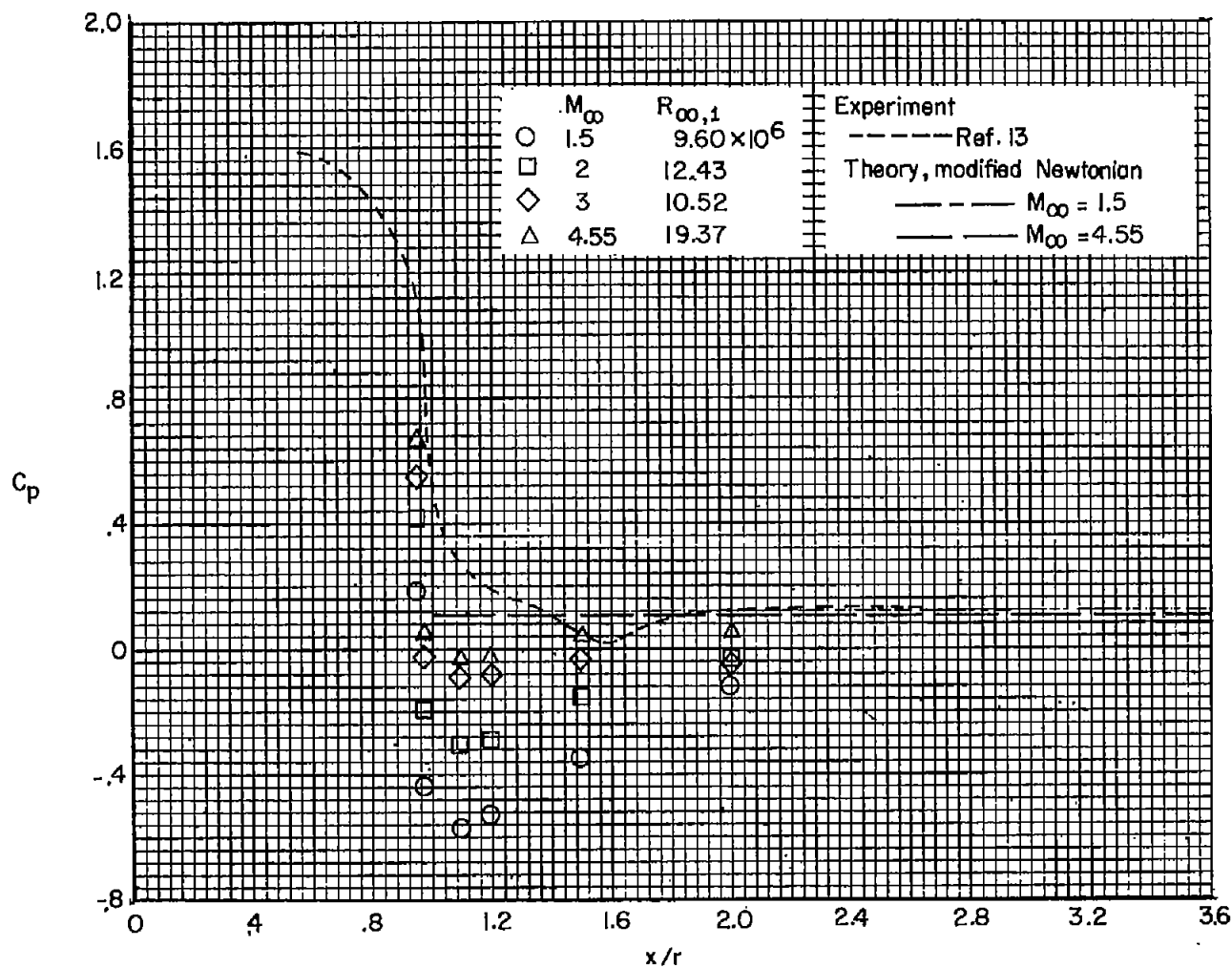
(b) Model B.

Figure 5.- Concluded.



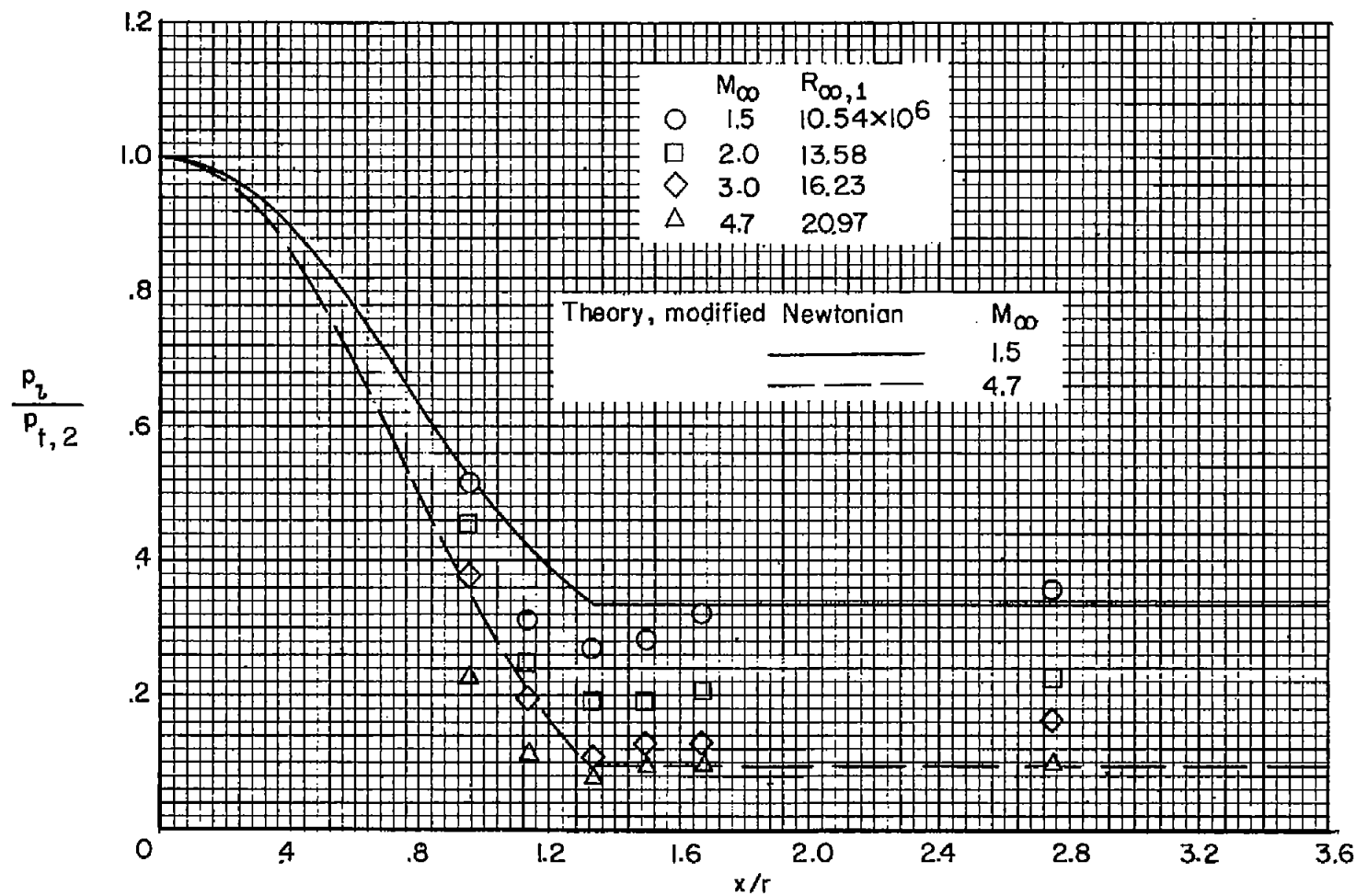
(a) Pressure ratios.

Figure 6.- Pressure measurements for model A.



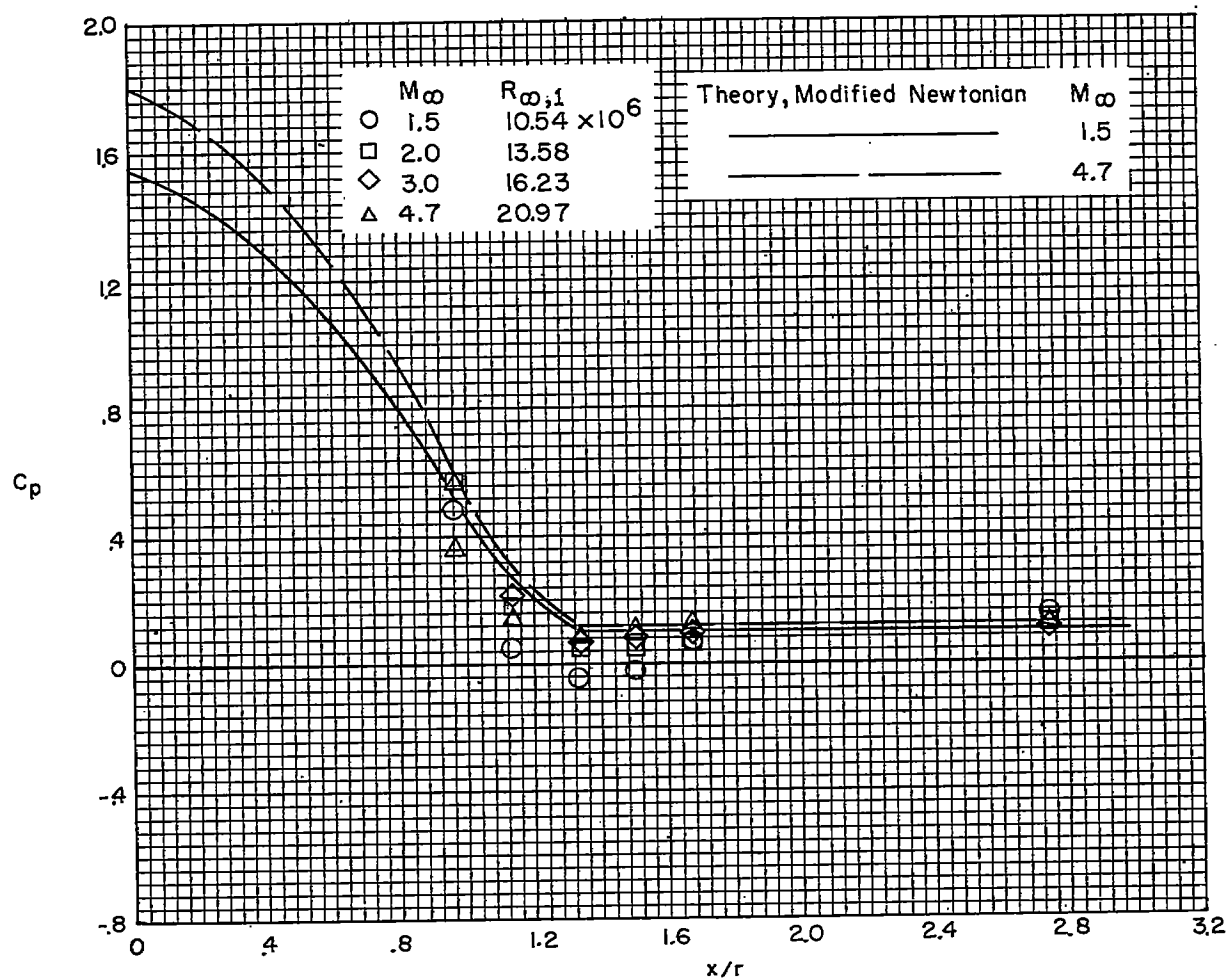
(b) Pressure coefficients.

Figure 6.- Concluded.



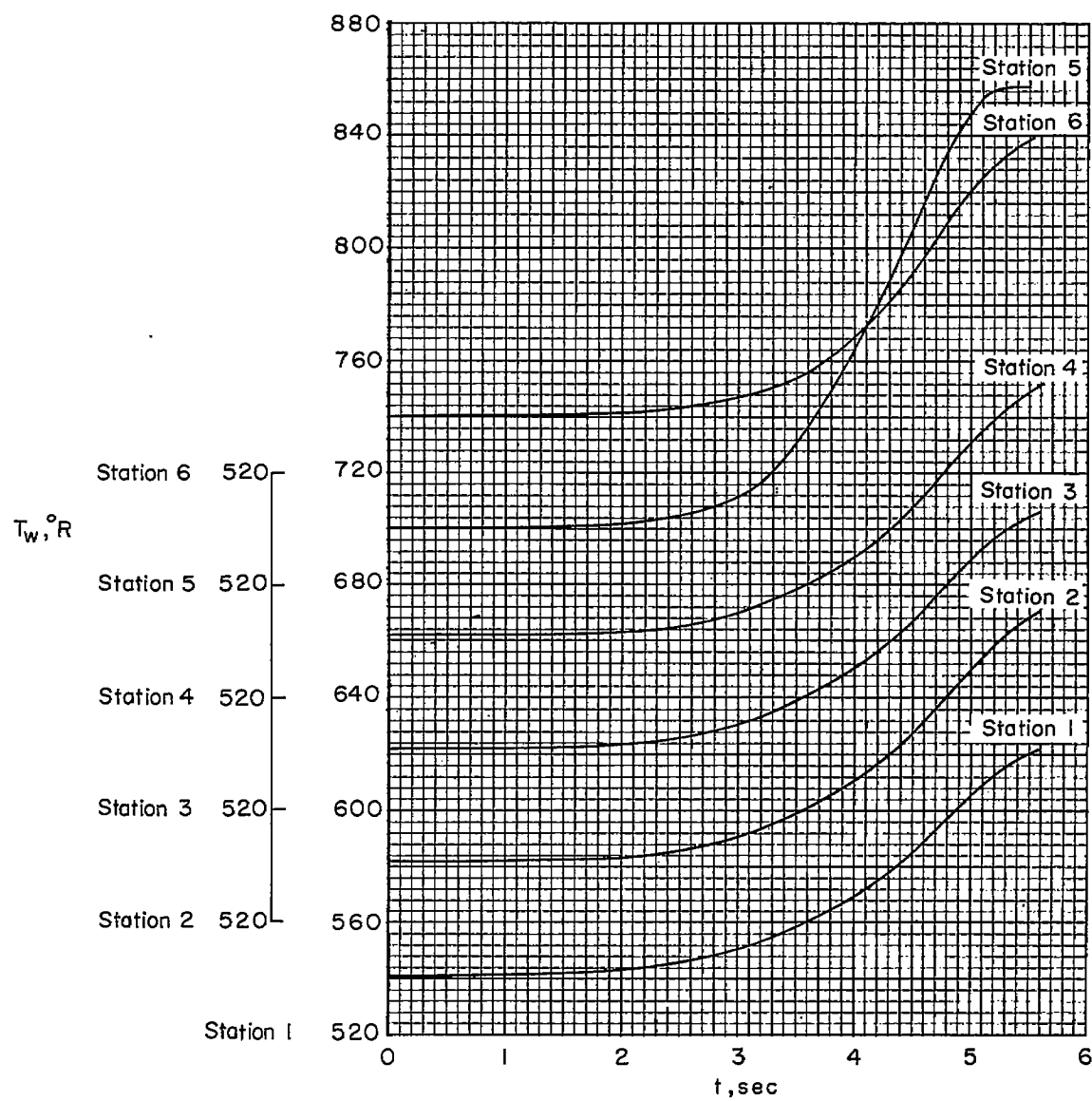
(a) Pressure ratios.

Figure 7.- Pressure measurements for model B.



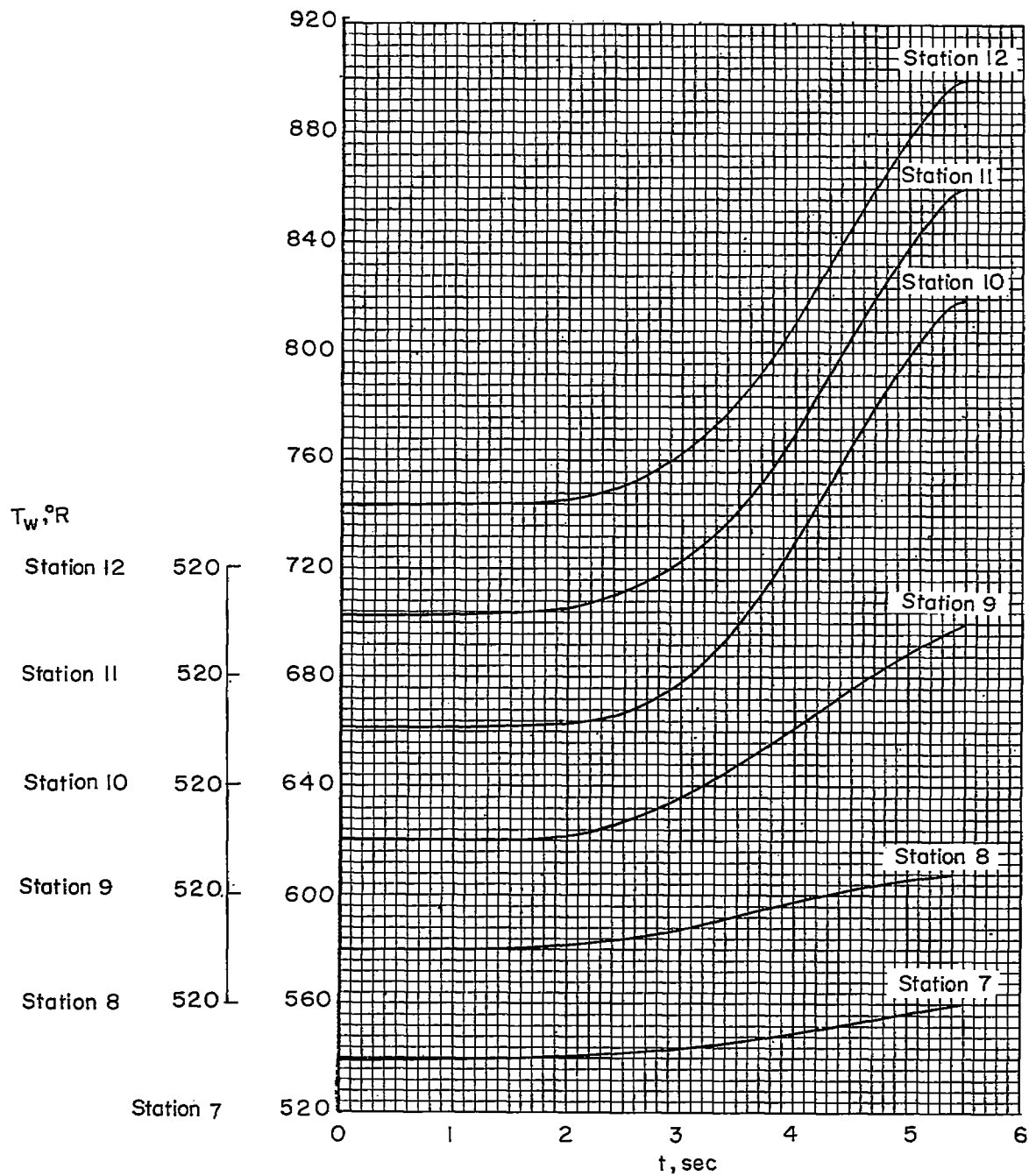
(b) Pressure coefficients.

Figure 7.- Concluded.



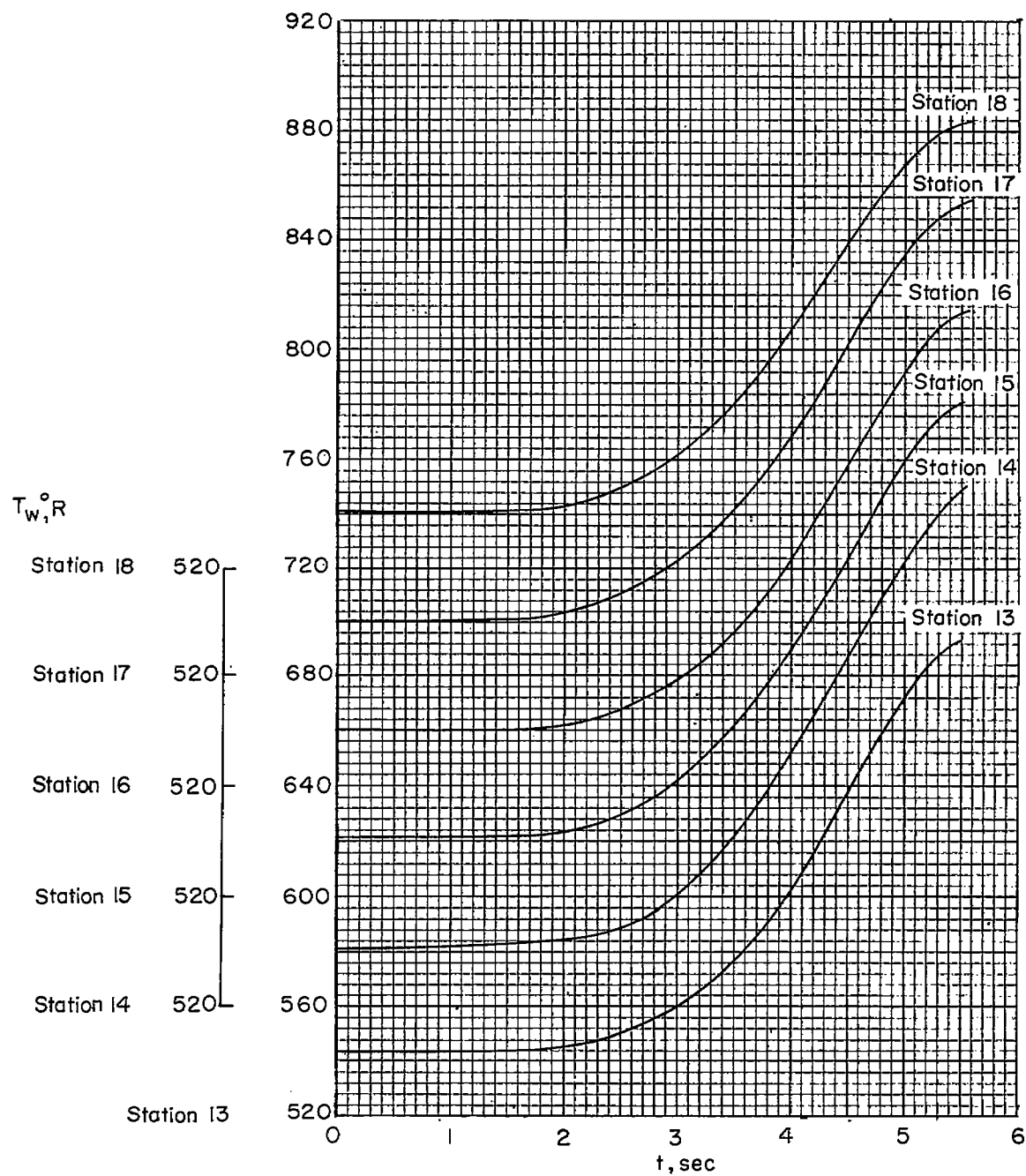
(a) Thermocouples 1 to 6.

Figure 8.- Skin-temperature time histories for model A.



(b) Thermocouples 7 to 12.

Figure 8.- Continued.



(c) Thermocouples 13 to 18.

Figure 8.- Concluded.

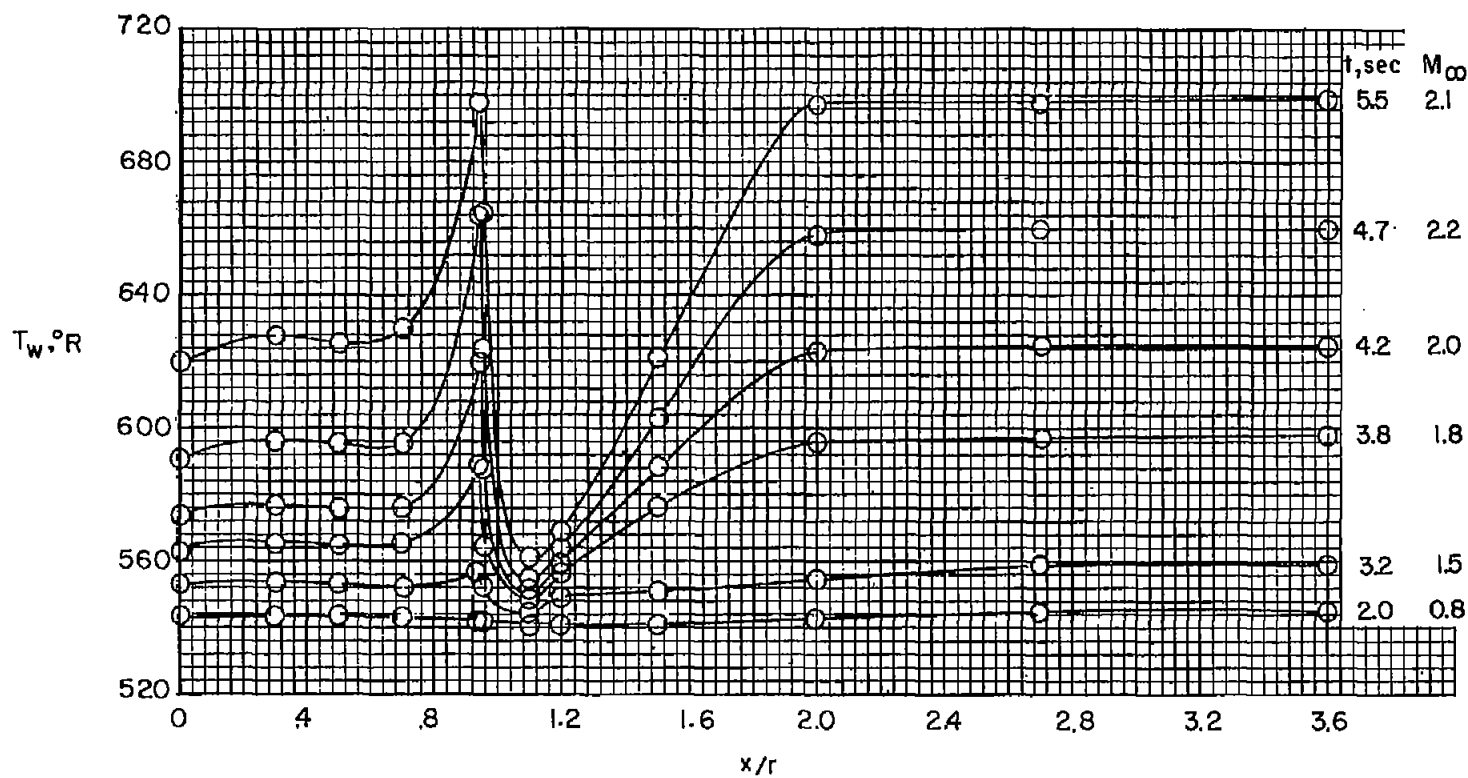
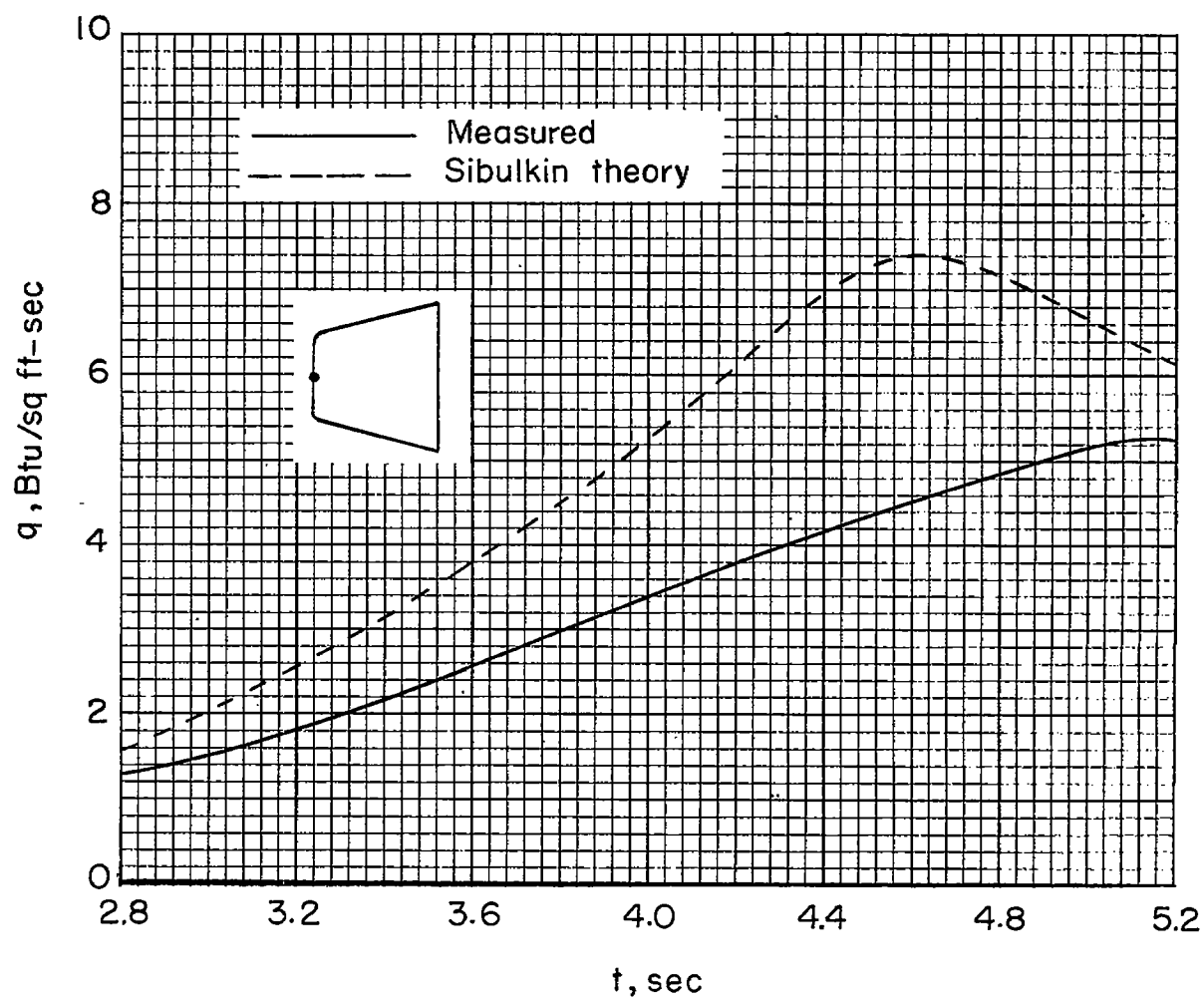
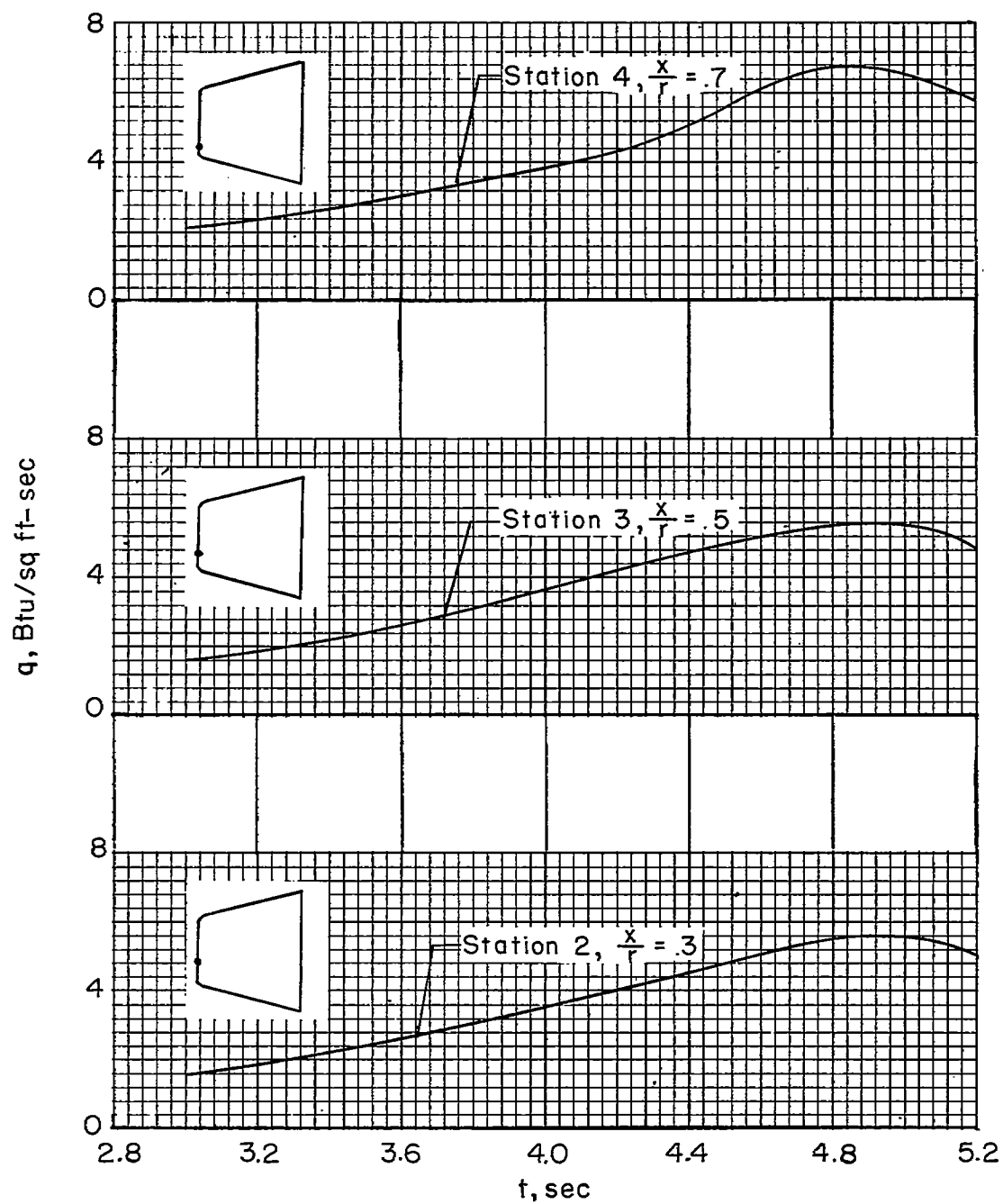


Figure 9.- Skin temperatures along the surface for several Mach numbers. Model A.



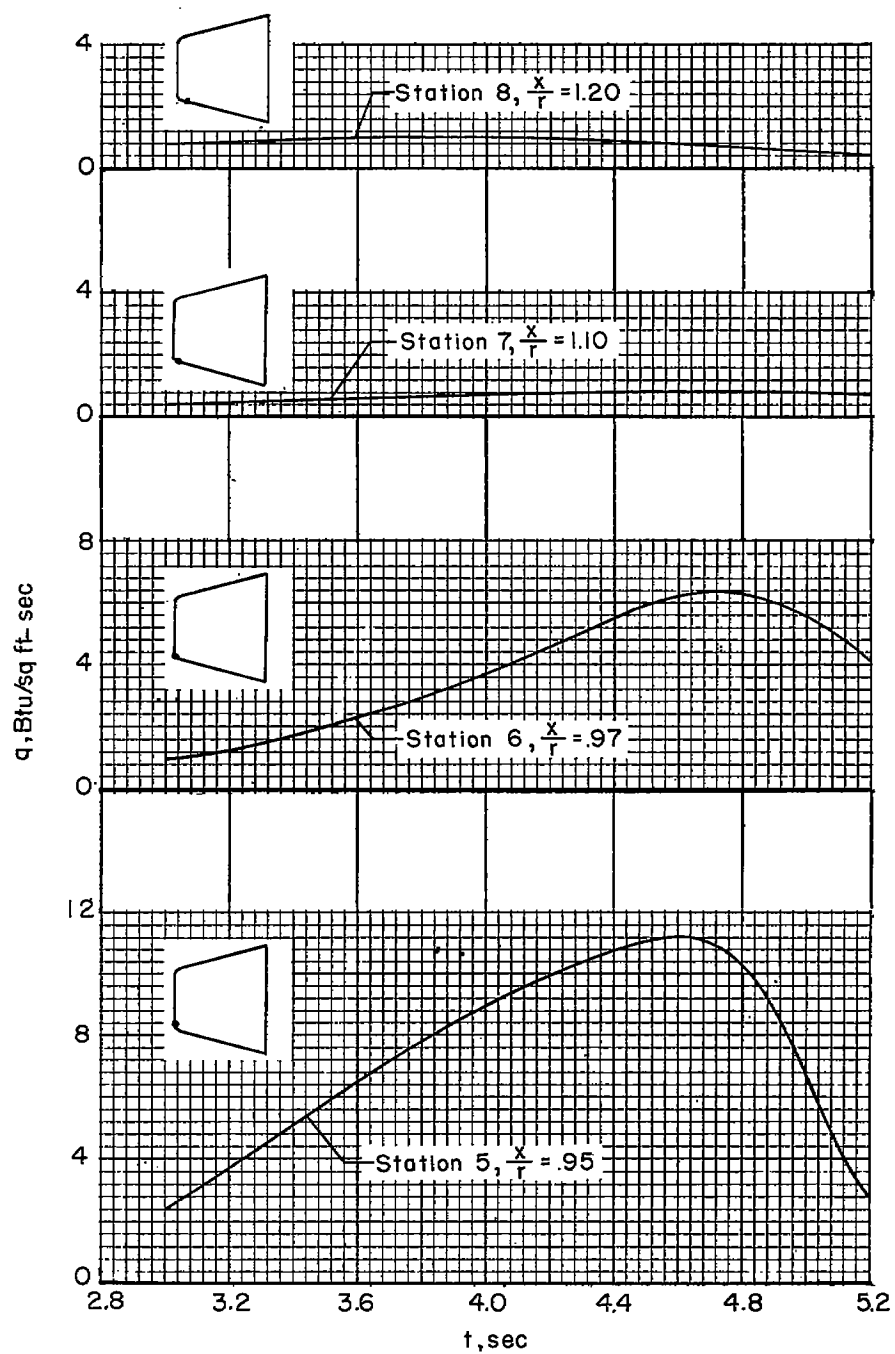
(a) Station 1, stagnation point, $\frac{x}{r} = 0$.

Figure 10.- Measured heating rates for model A.



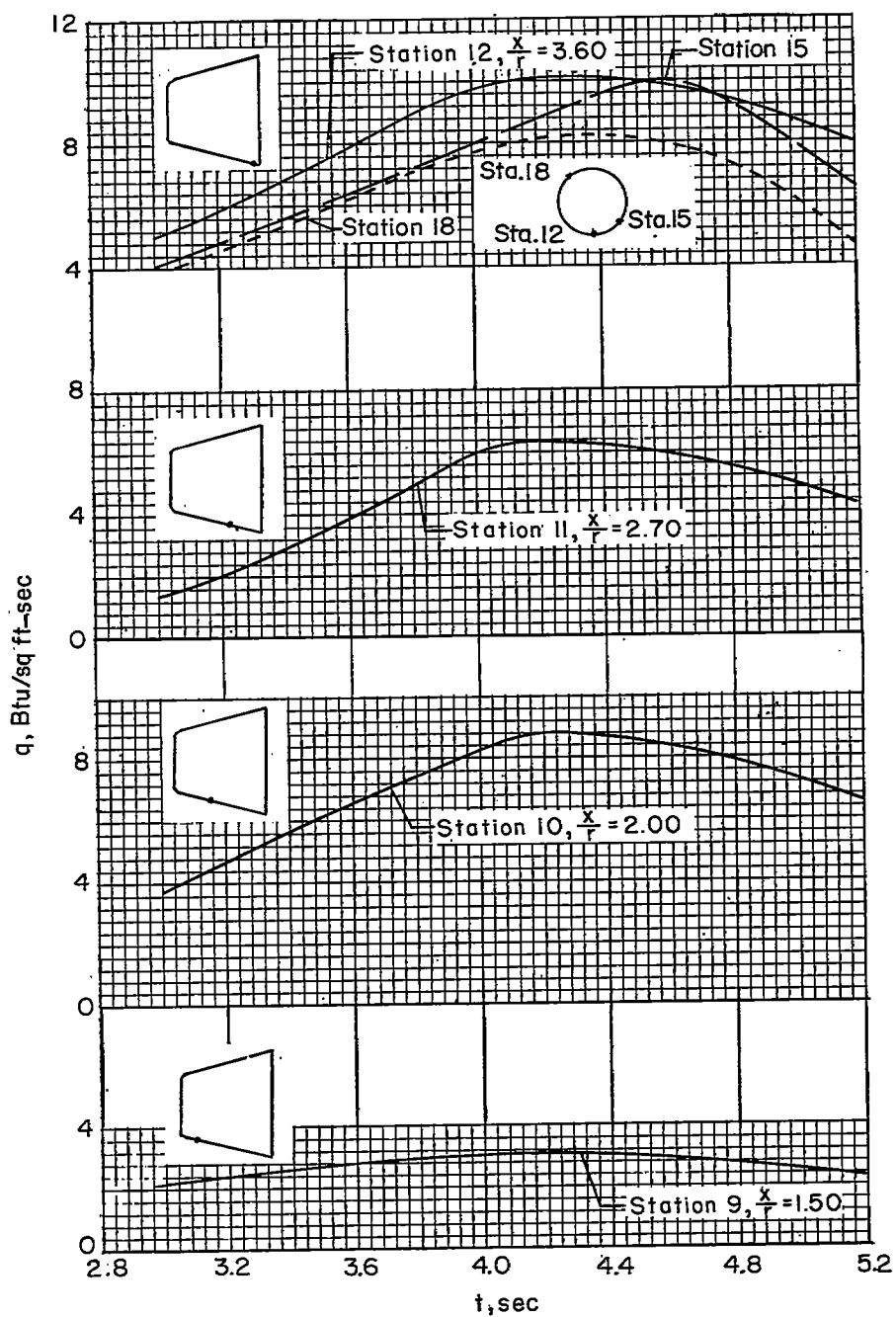
(b) Stations 2, 3, and 4.

Figure 10.- Continued.



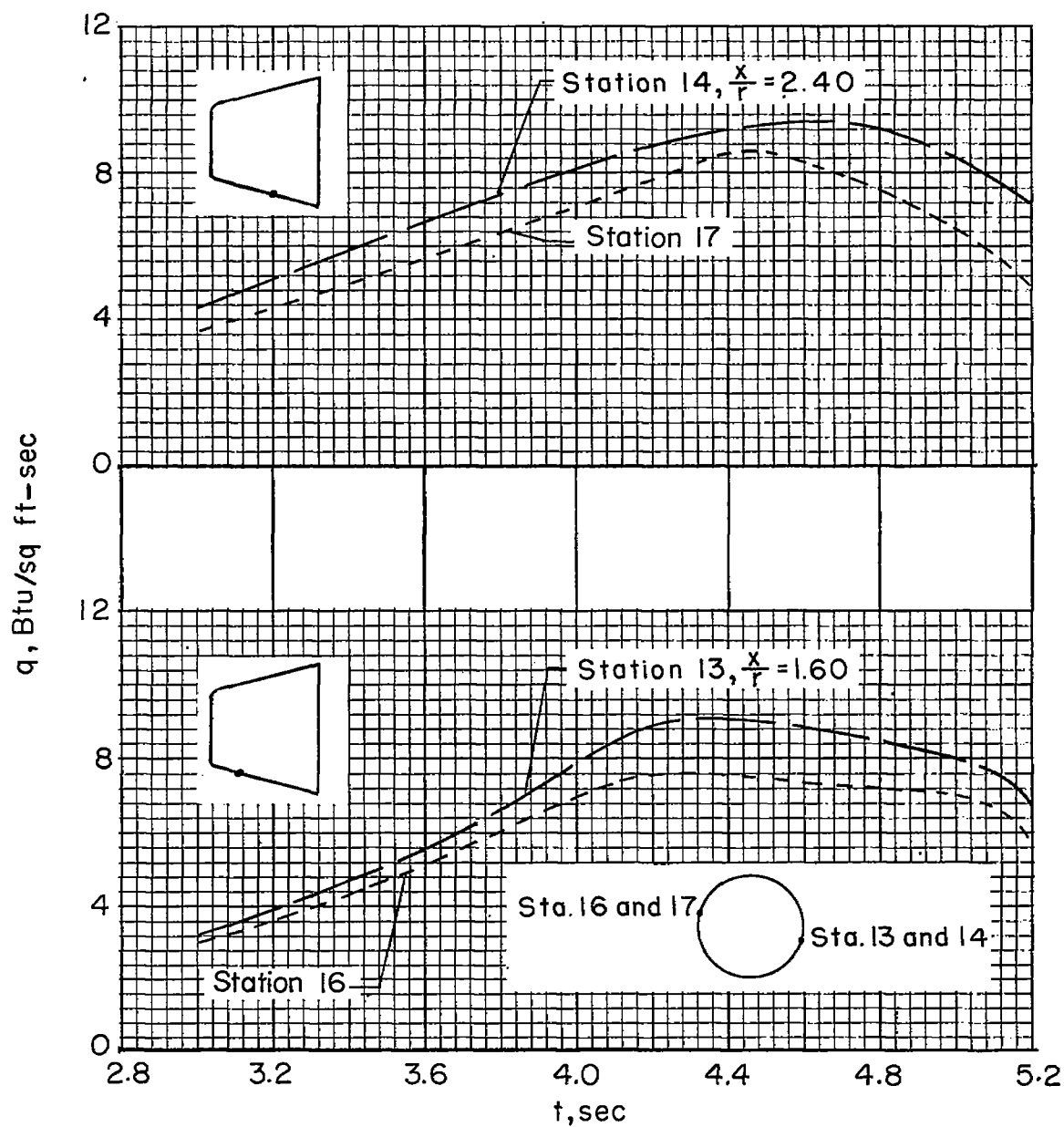
(c) Stations 5, 6, 7, and 8.

Figure 10.- Continued.



(d) Stations 9, 10, 11, 12, 15, and 18.

Figure 10.- Continued.



(e) Stations 13, 14, 16, and 17.

Figure 10.- Concluded.

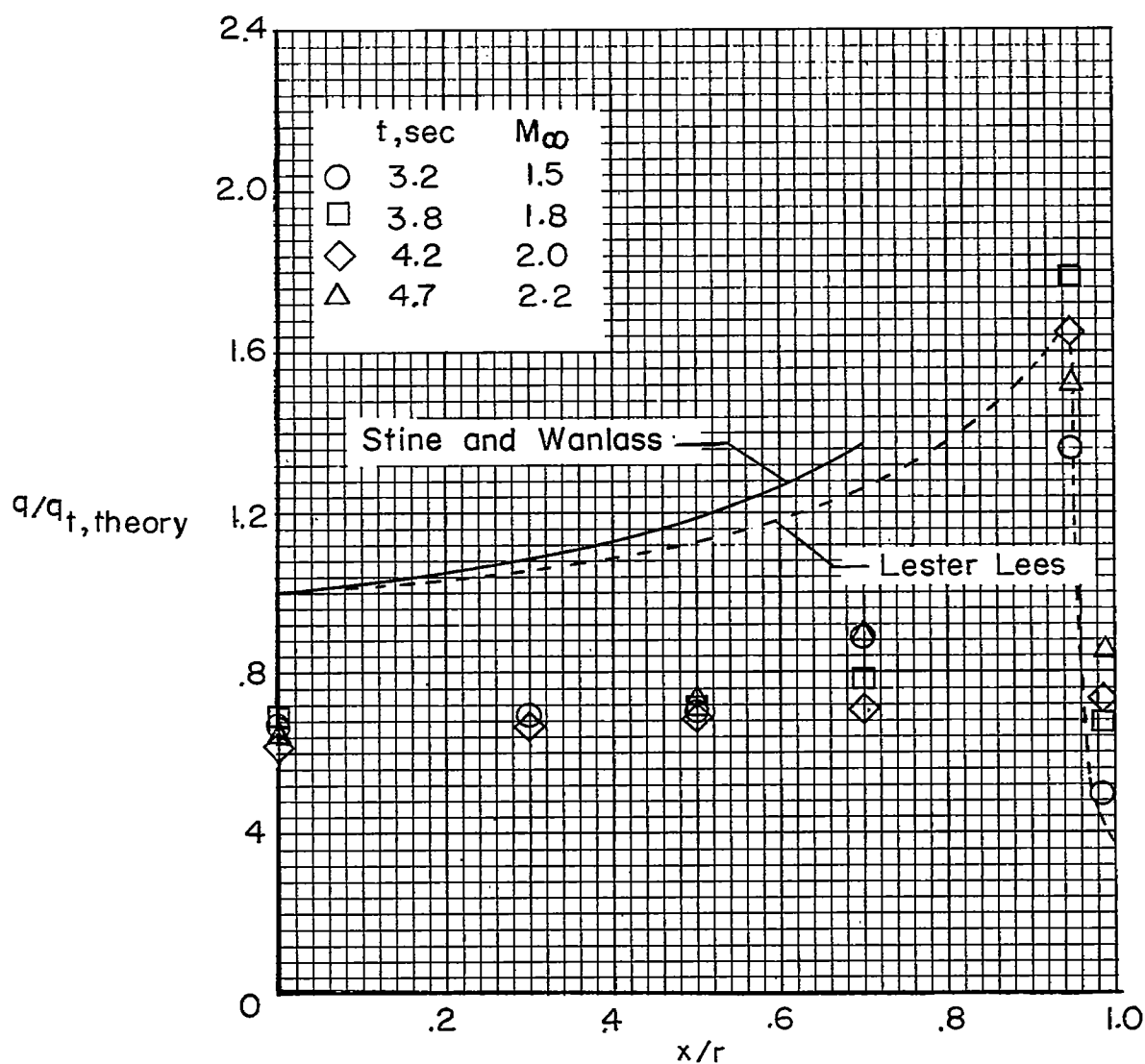


Figure 11.- Ratio of measured heating rate to theoretical heating rate at the stagnation point for the flat face of model A.

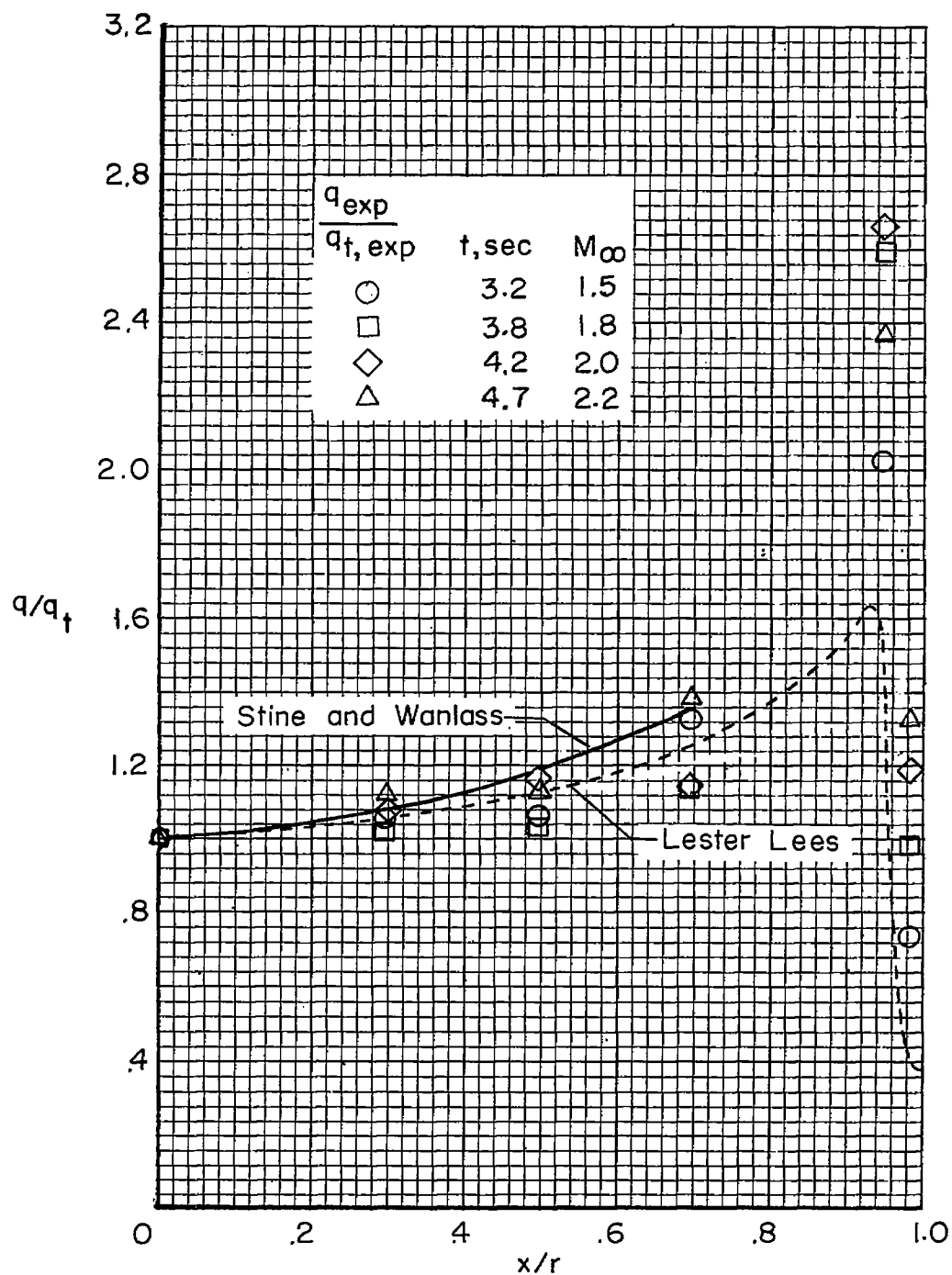
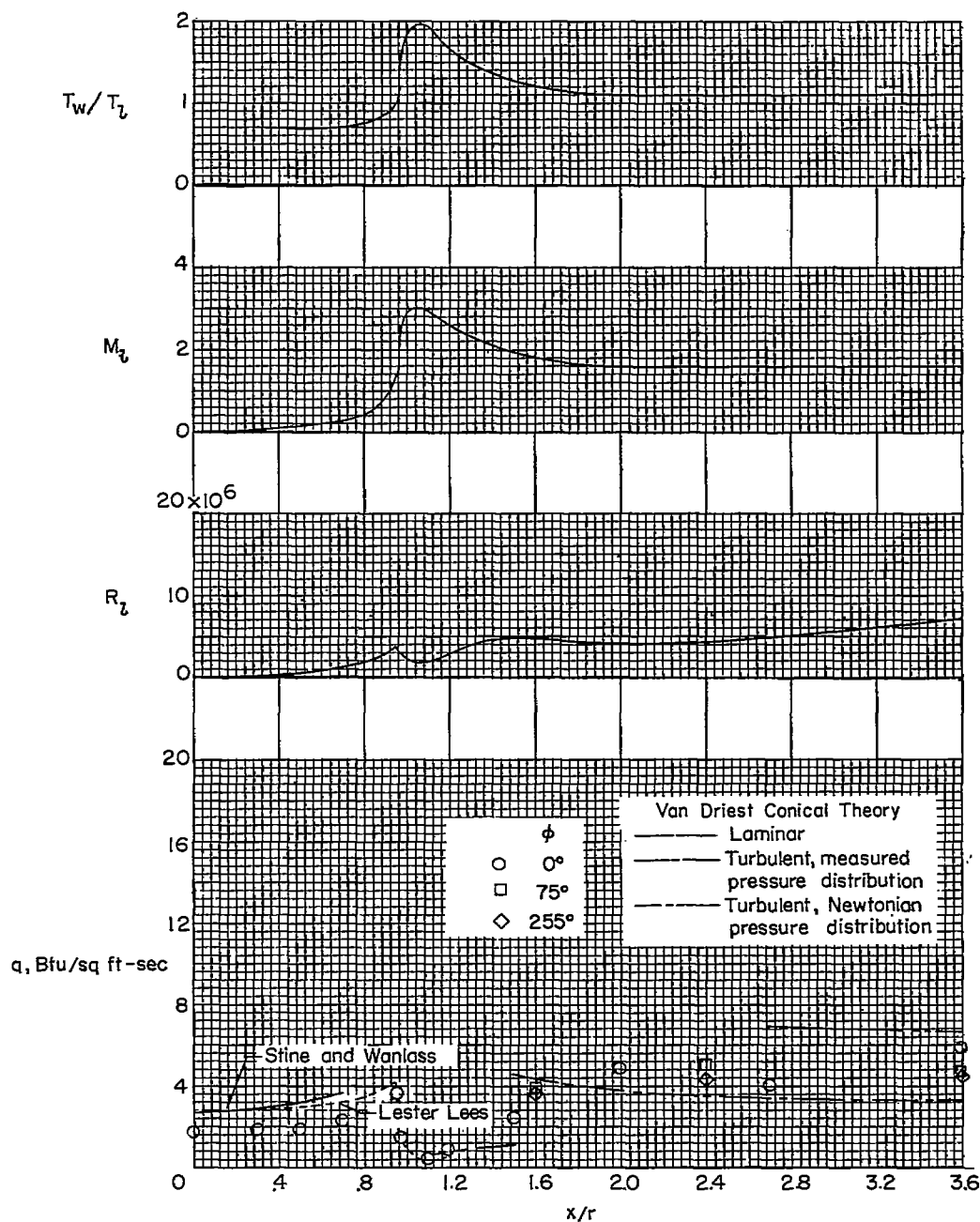
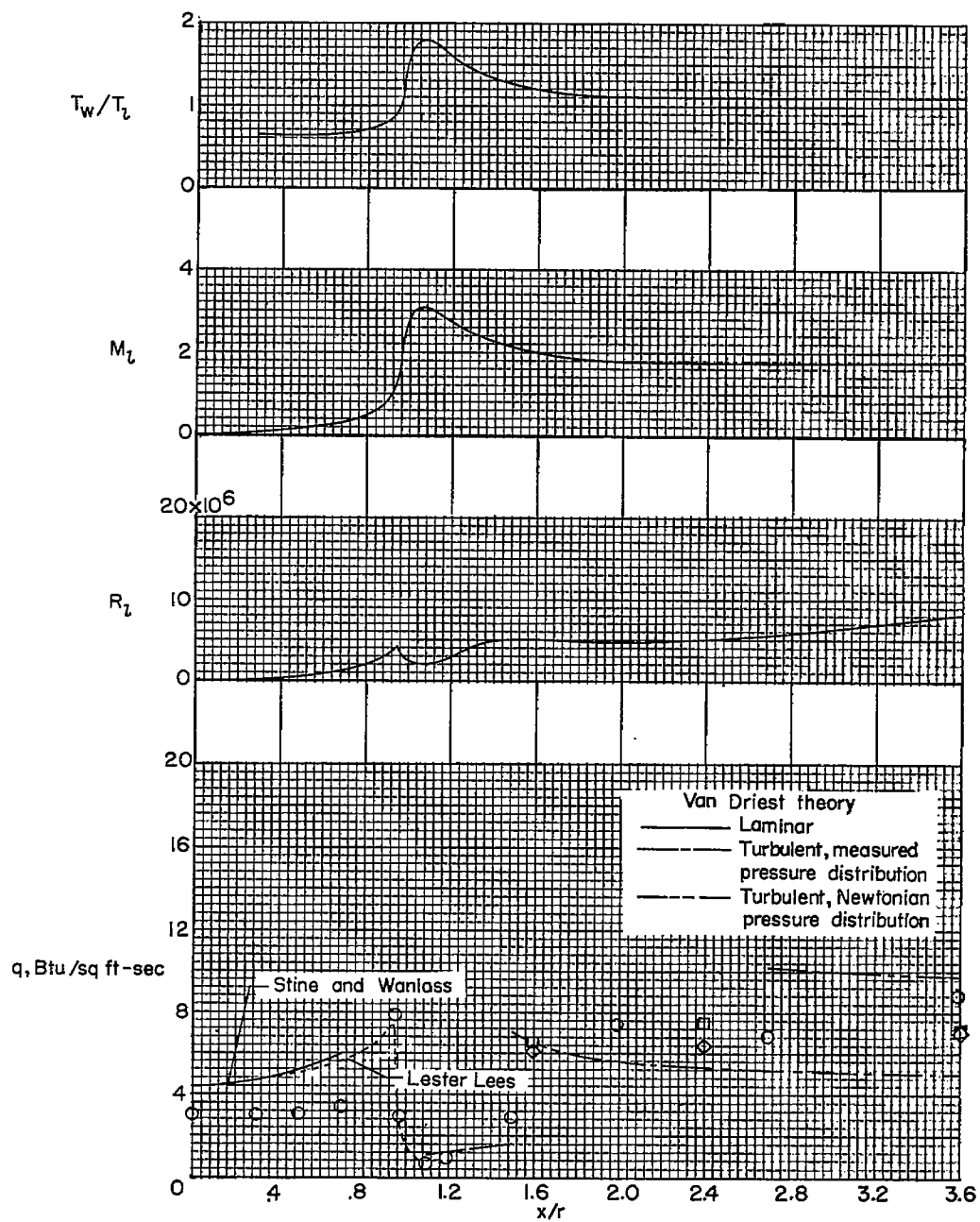


Figure 12.- Ratio of measured heating rate to measured heating rate at the stagnation point for the flat face of model A.



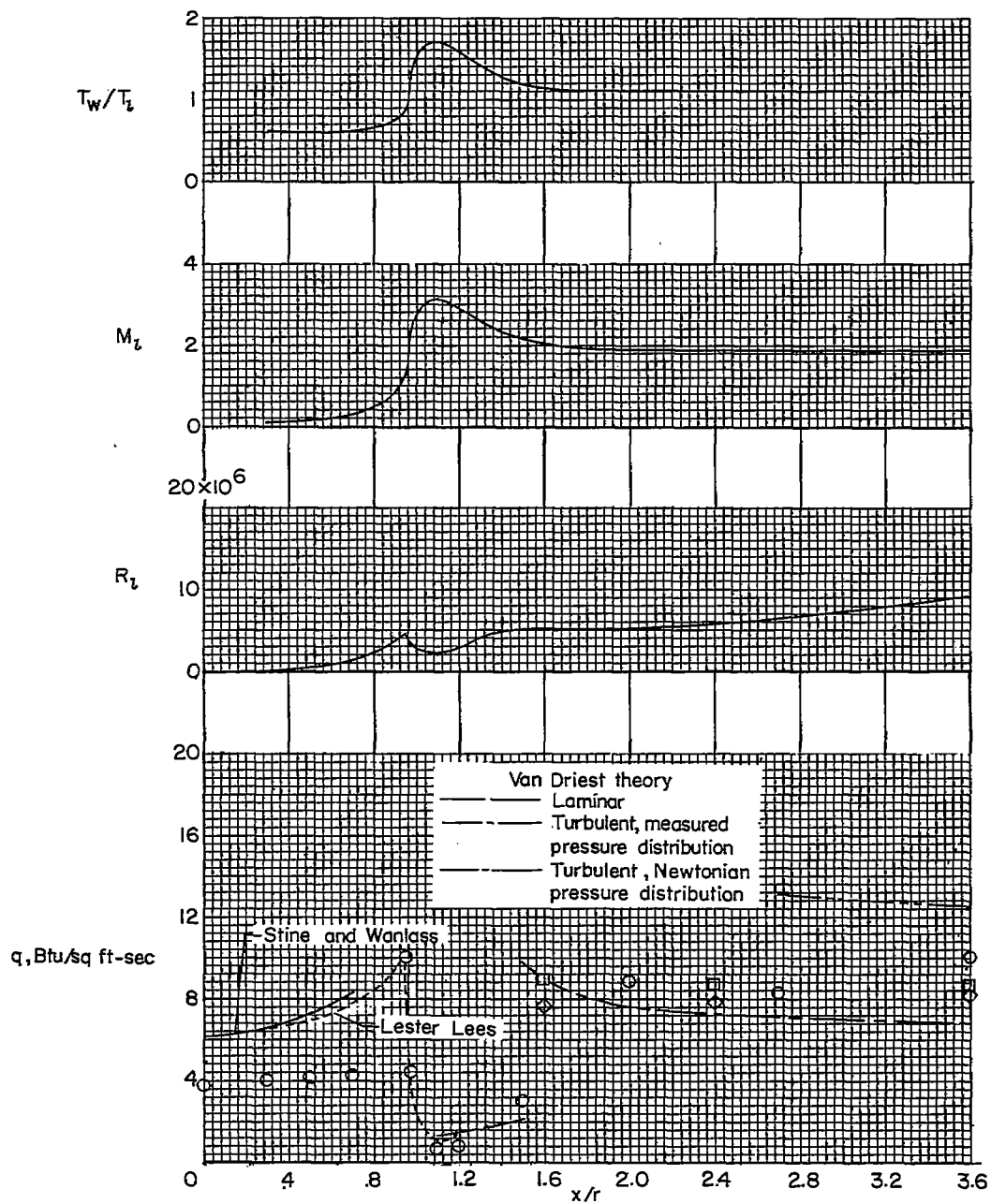
(a) $t = 3.2$ seconds; $M_\infty = 1.5$.

Figure 13.- Local heating rates, Reynolds number, Mach number, and ratio of wall temperature to local static temperature for model A.



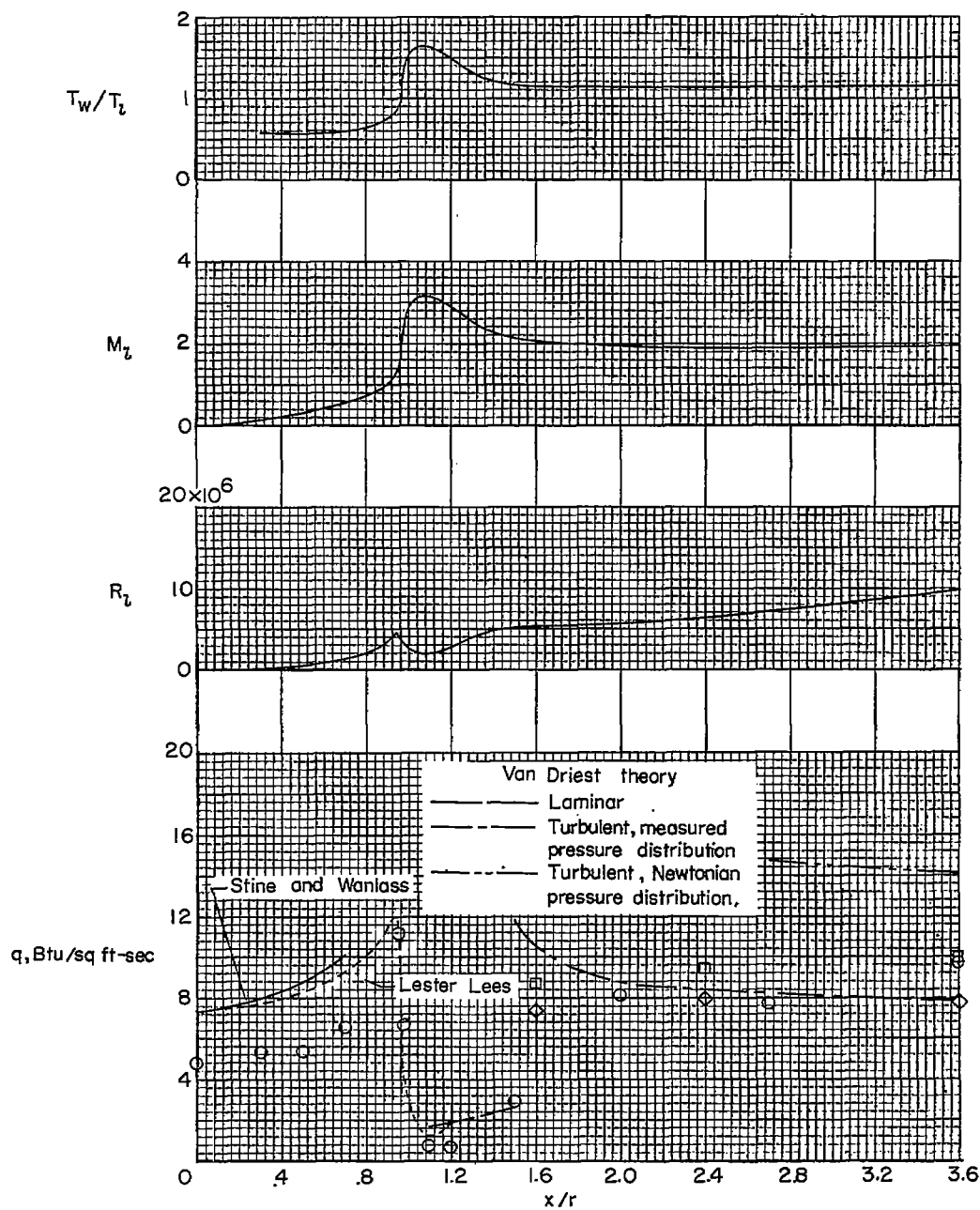
(b) $t = 3.8$ seconds; $M_\infty = 1.8$.

Figure 13.- Continued.



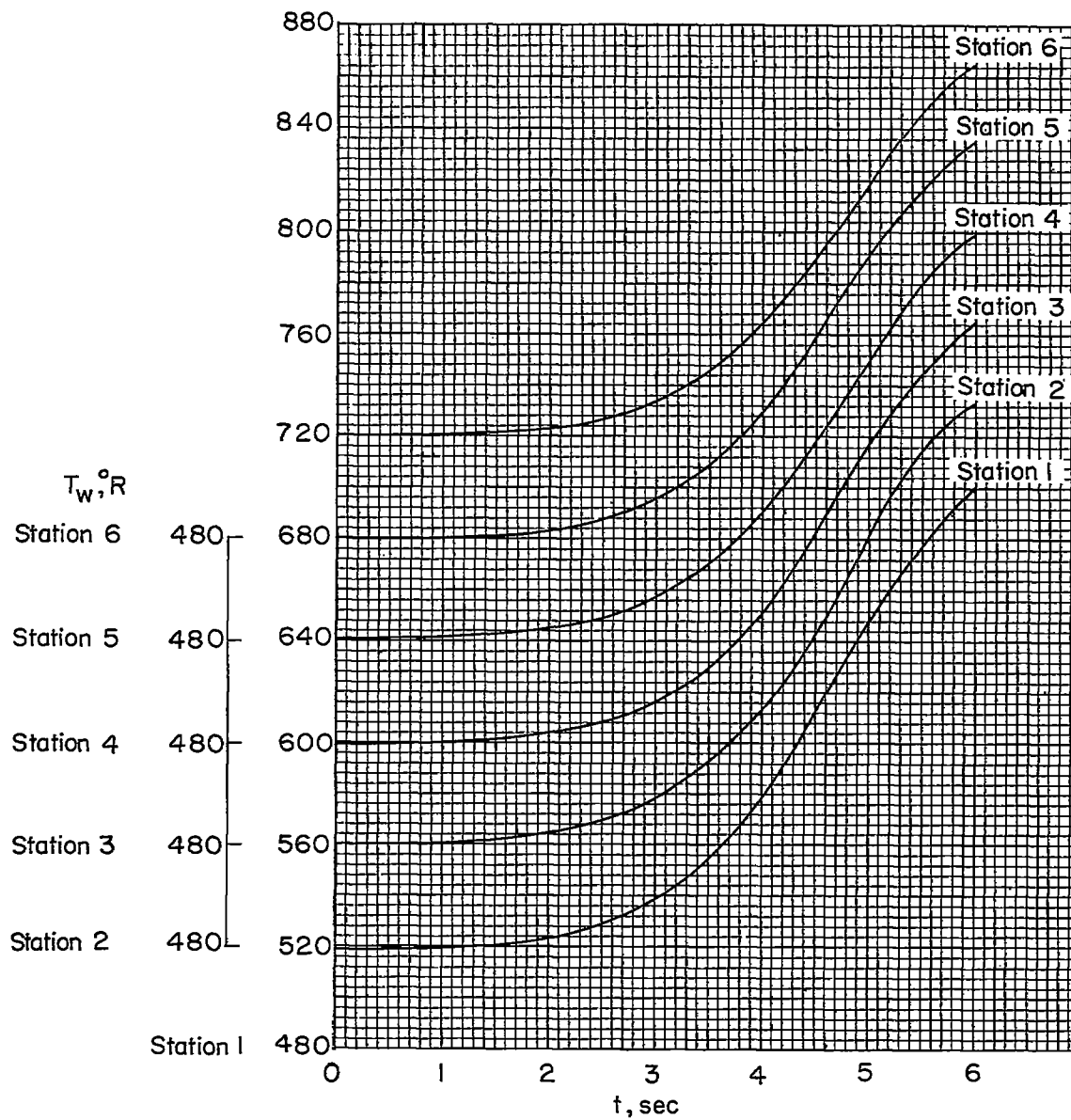
(c) $t = 4.2$ seconds; $M_\infty = 2.0$.

Figure 13.- Continued.



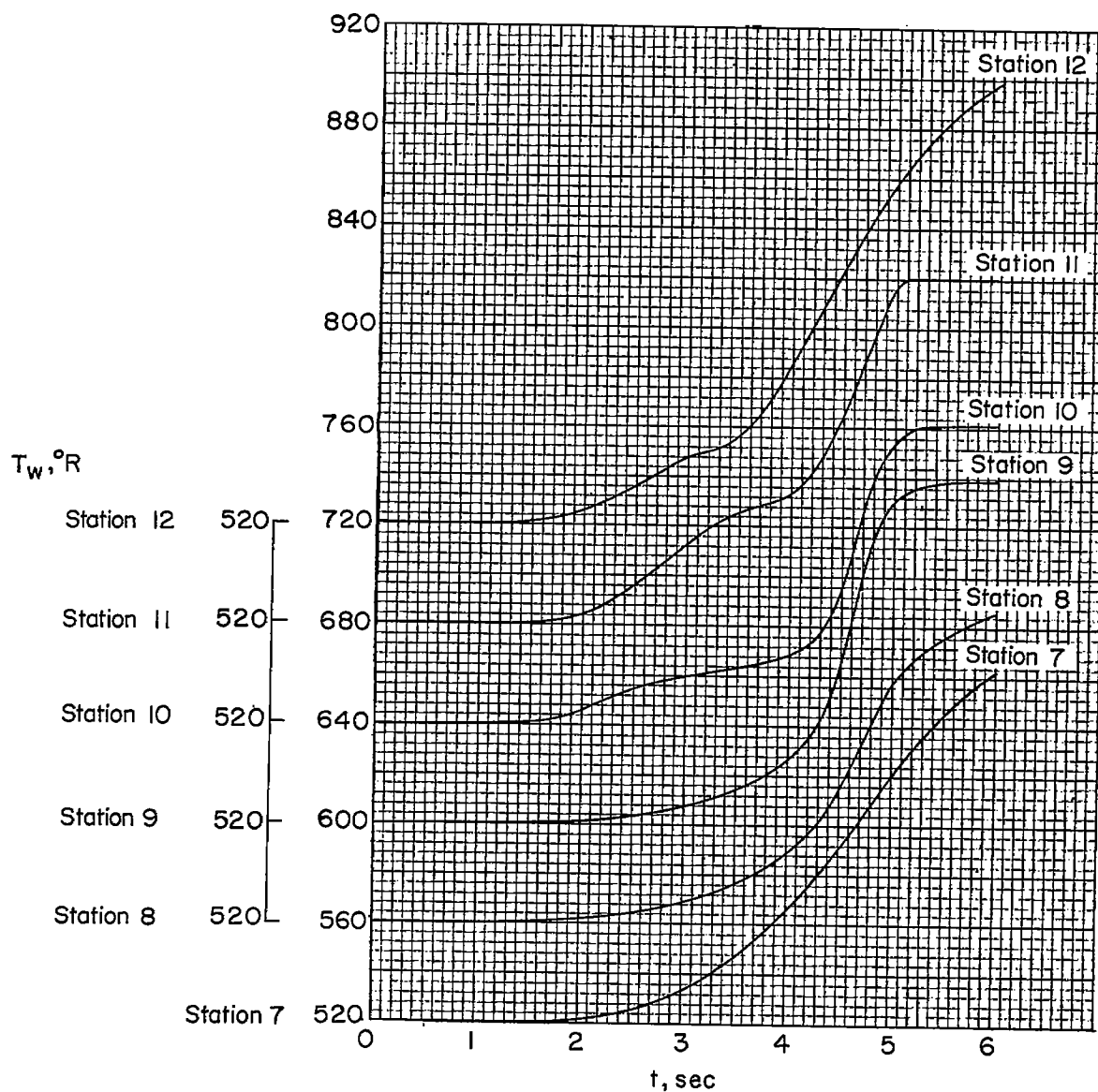
(d) $t = 4.7$ seconds; $M_\infty = 2.2$.

Figure 13.- Concluded.



(a) Thermocouples 1 to 6.

Figure 14.- Skin-temperature time histories for model B.



(b) Thermocouples 7 to 12.

Figure 14.- Concluded.

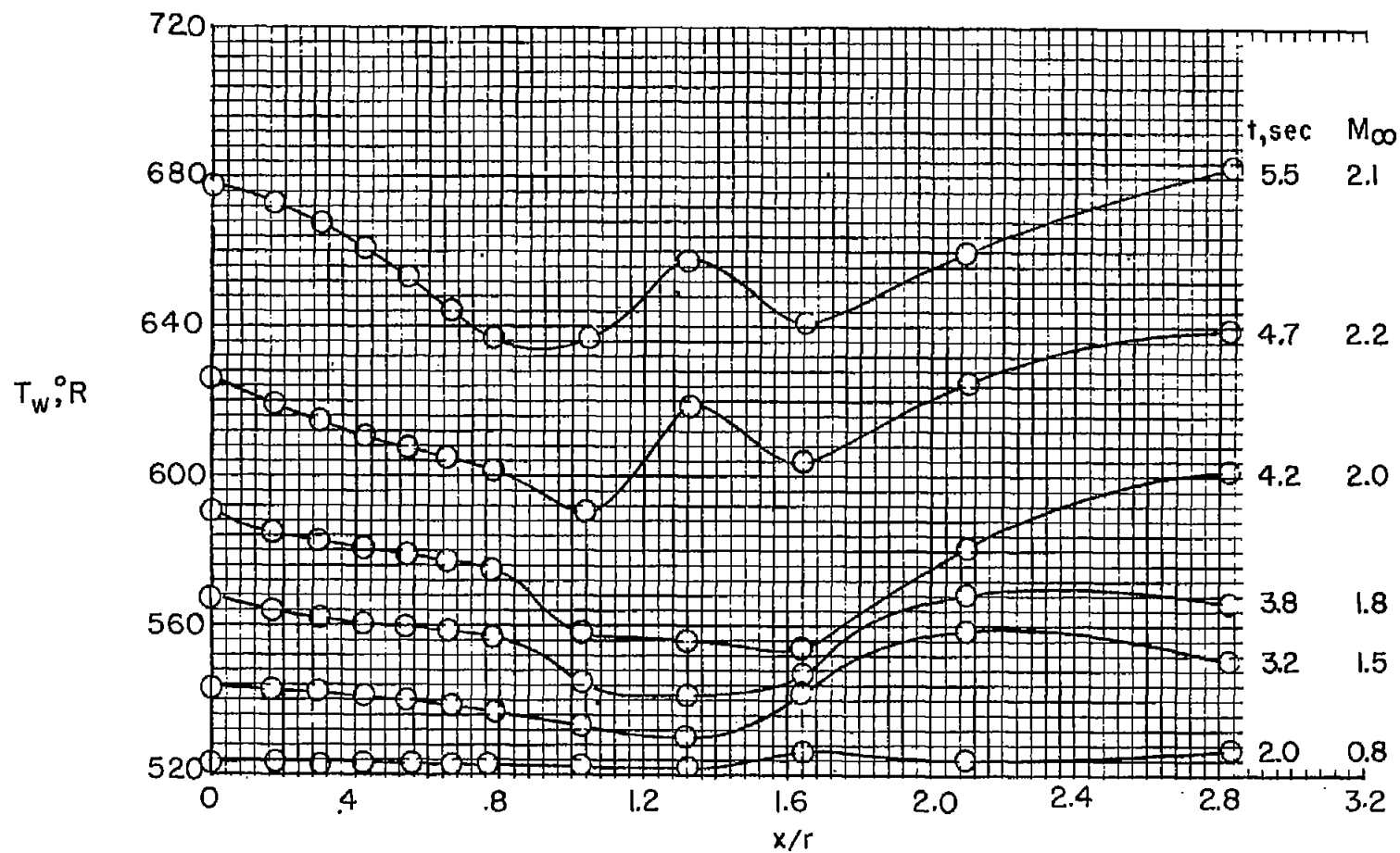
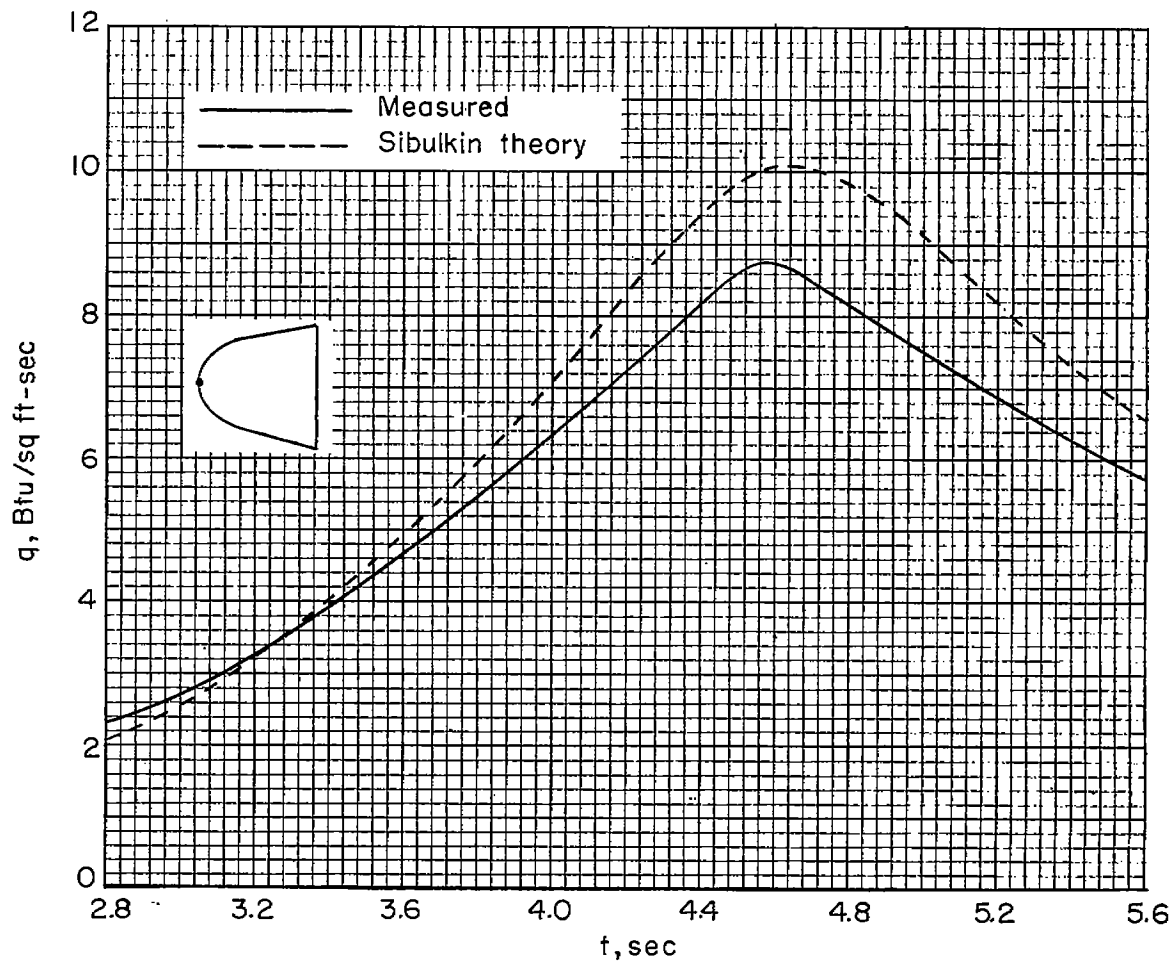
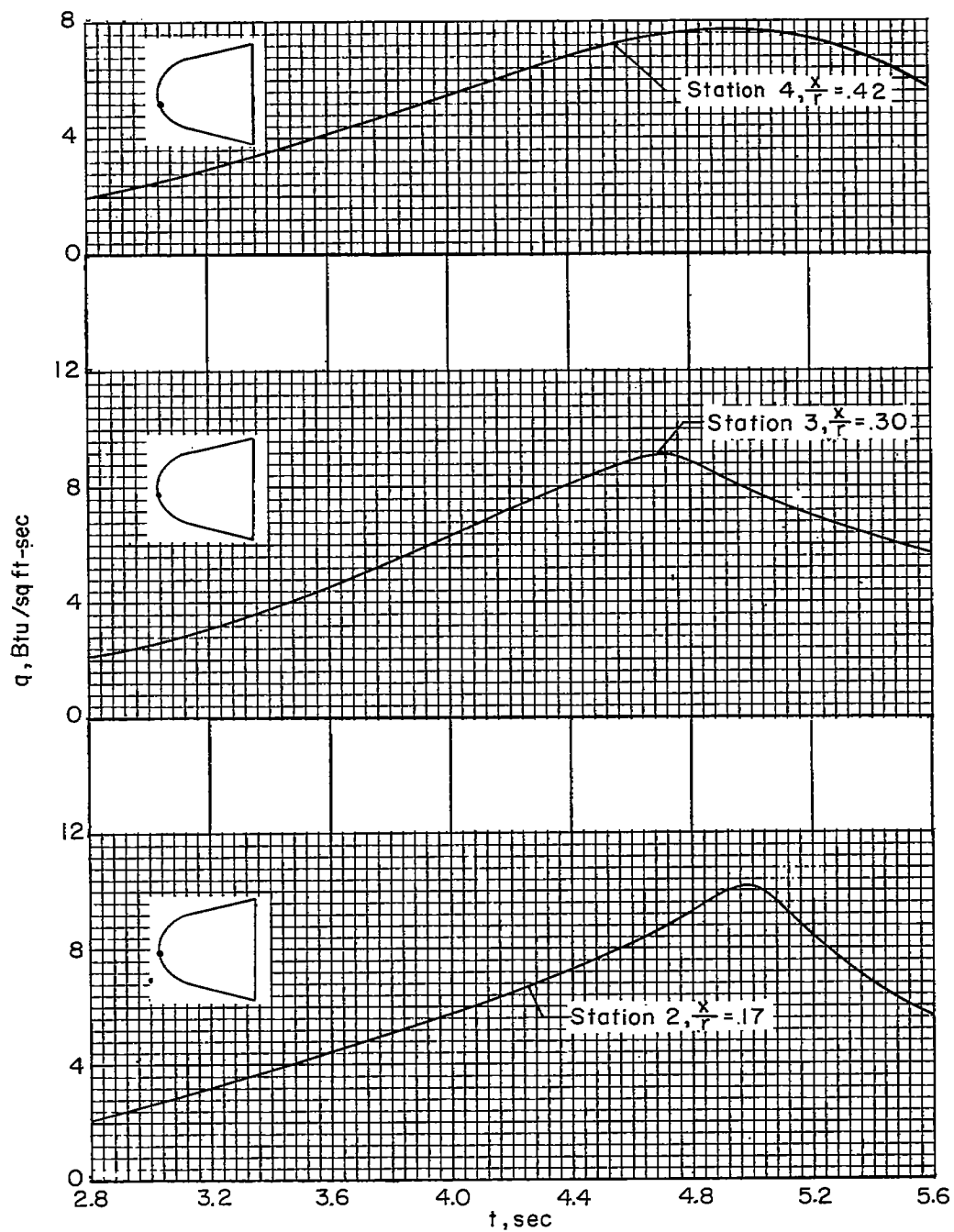


Figure 15.- Skin temperatures along the surface for several Mach numbers. Model B.



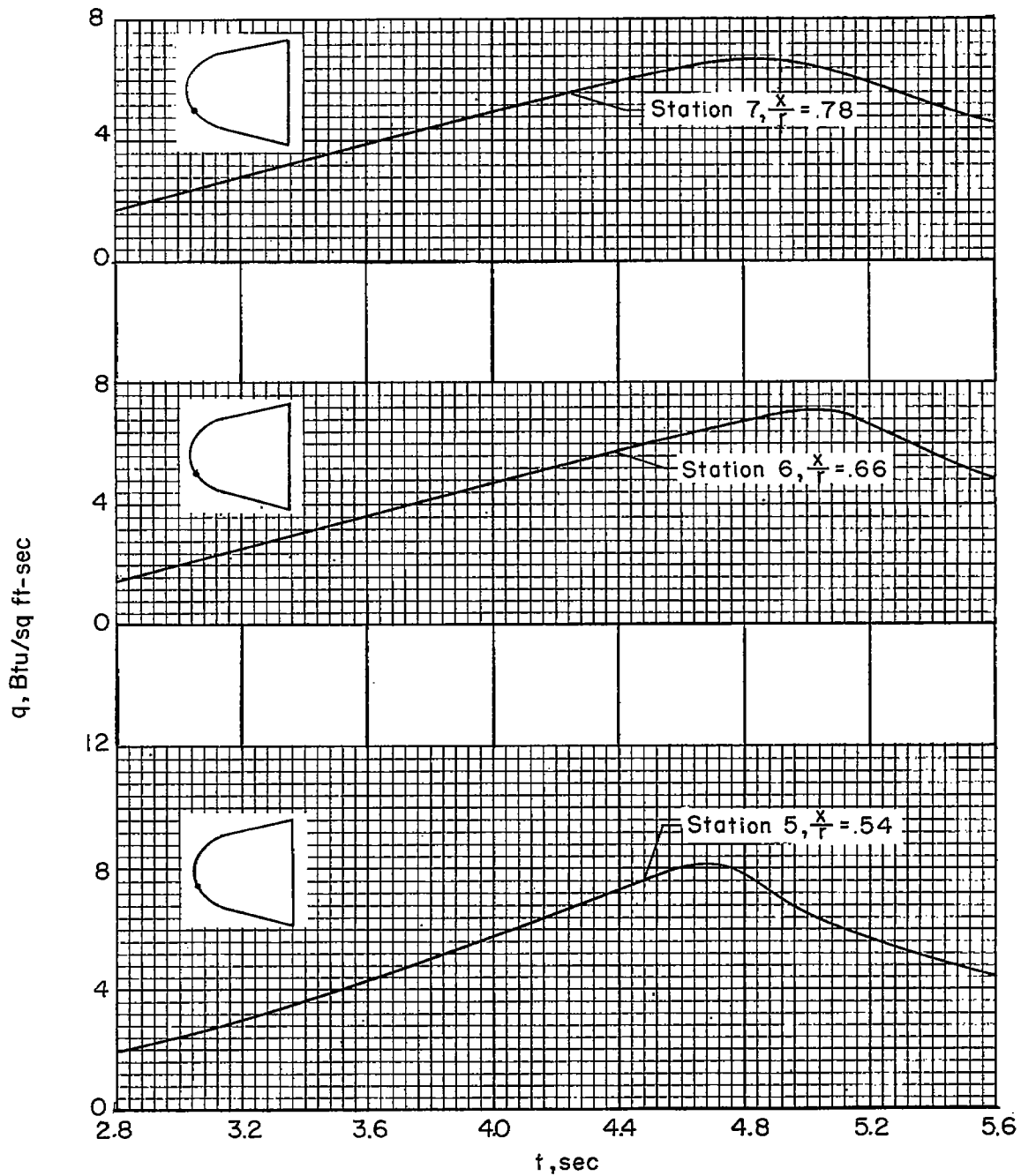
(a) Station 1, stagnation point, $\frac{x}{r} = 0$.

Figure 16.- Measured heating rates for model B.



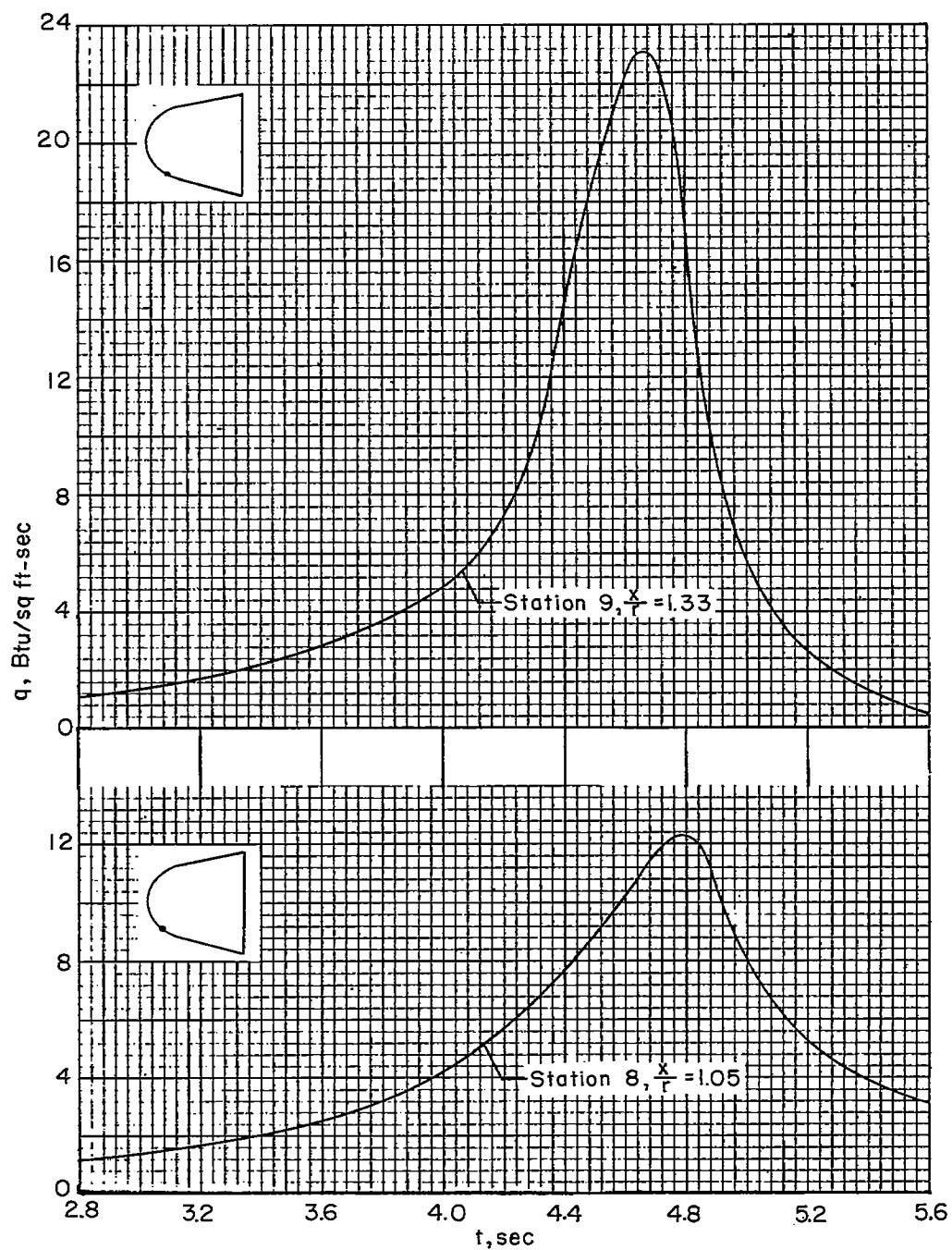
(b) Stations 2, 3, and 4.

Figure 16.- Continued.



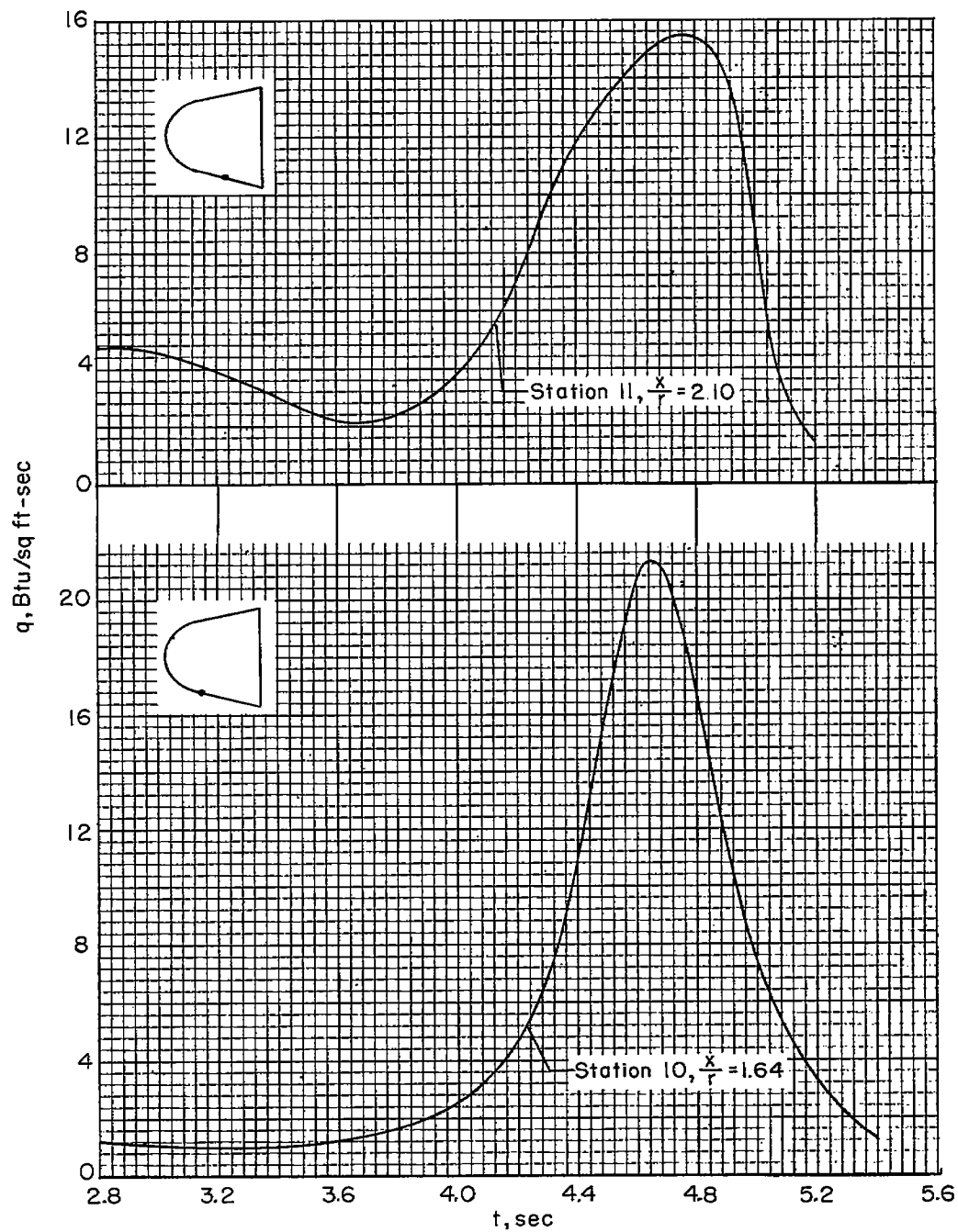
(c) Stations 5, 6, and 7.

Figure 16.- Continued.



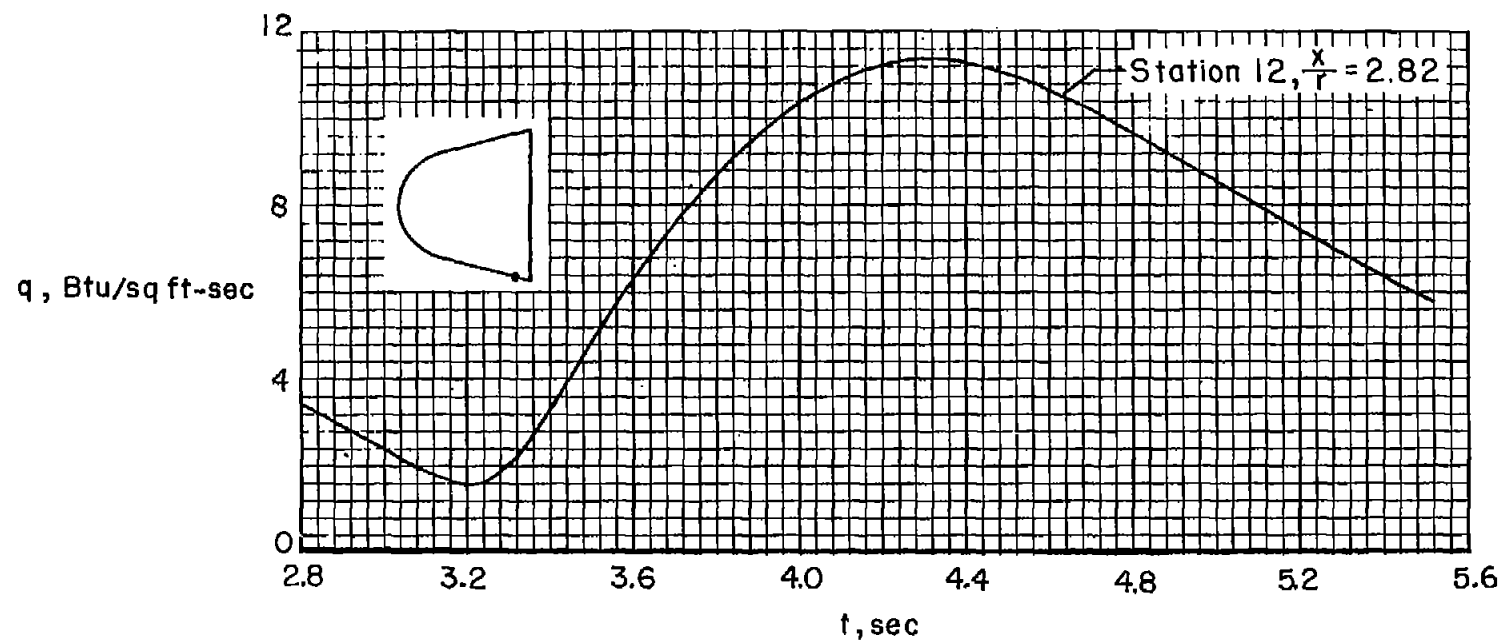
(d) Stations 8 and 9.

Figure 16.- Continued.



(e) Stations 10 and 11.

Figure 16.- Continued.



(f) Station 12.

Figure 16.- Concluded.

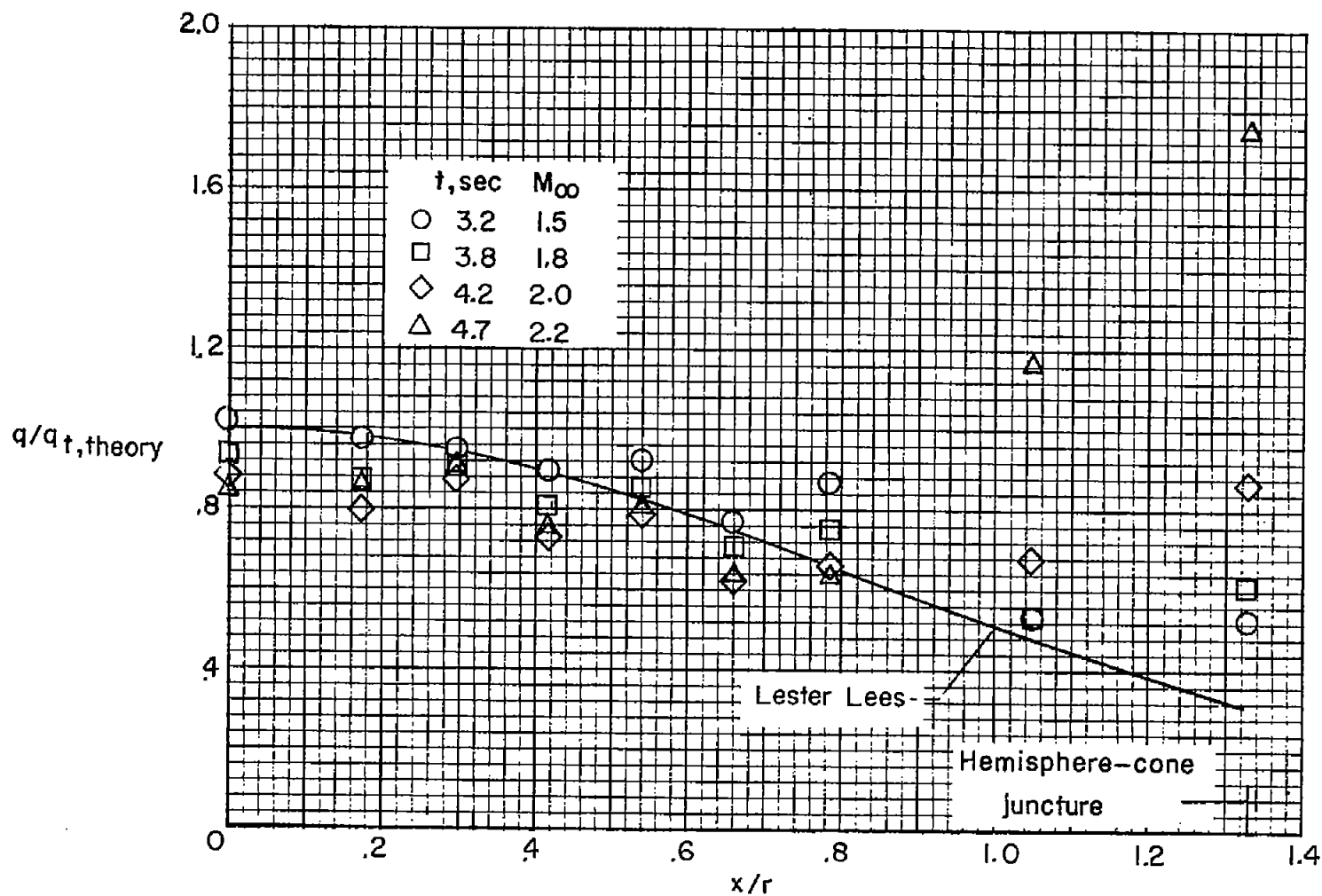


Figure 17.- Ratio of measured heating rate to theoretical heating rate at the stagnation point for the hemispherical portion of model B.

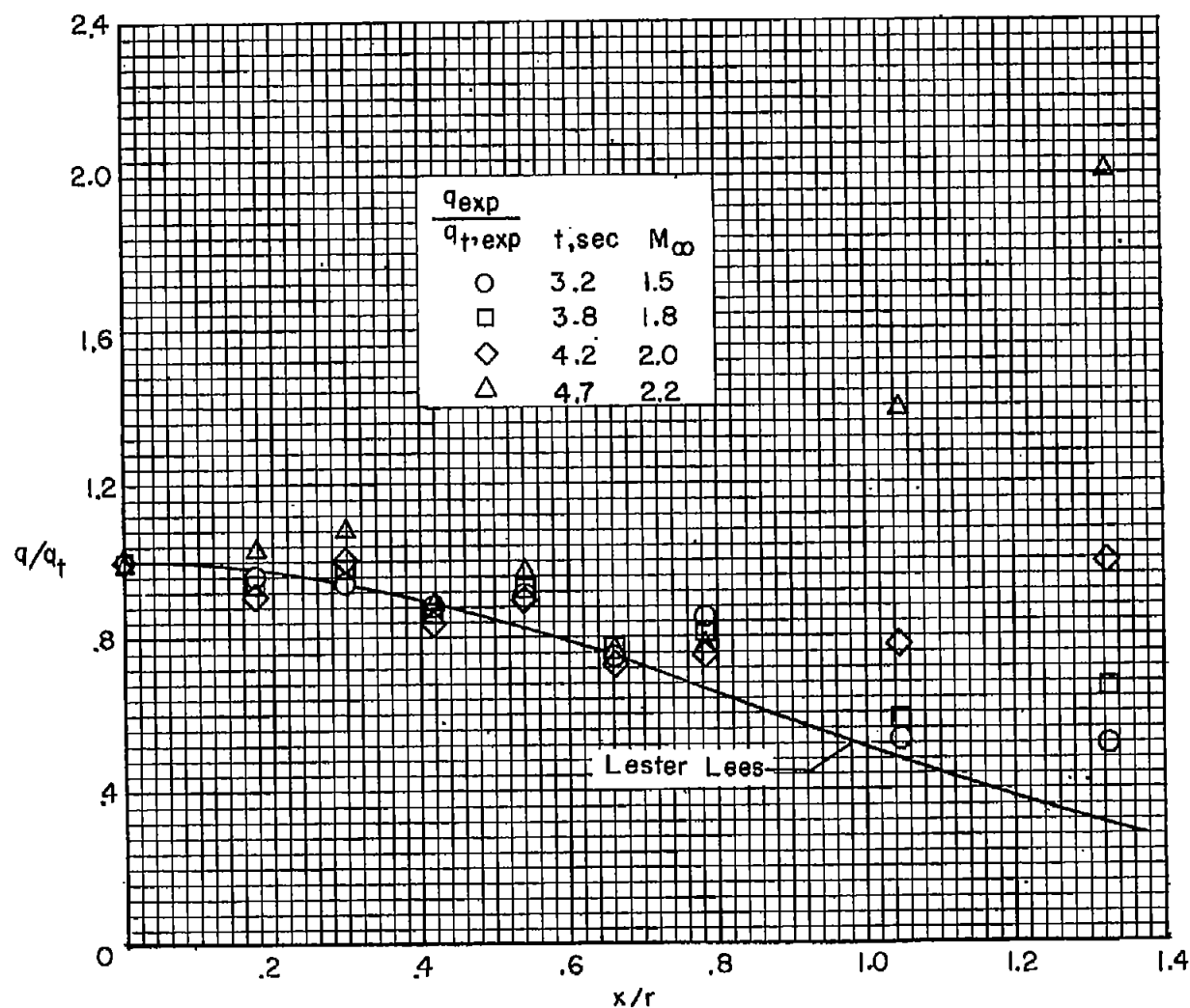
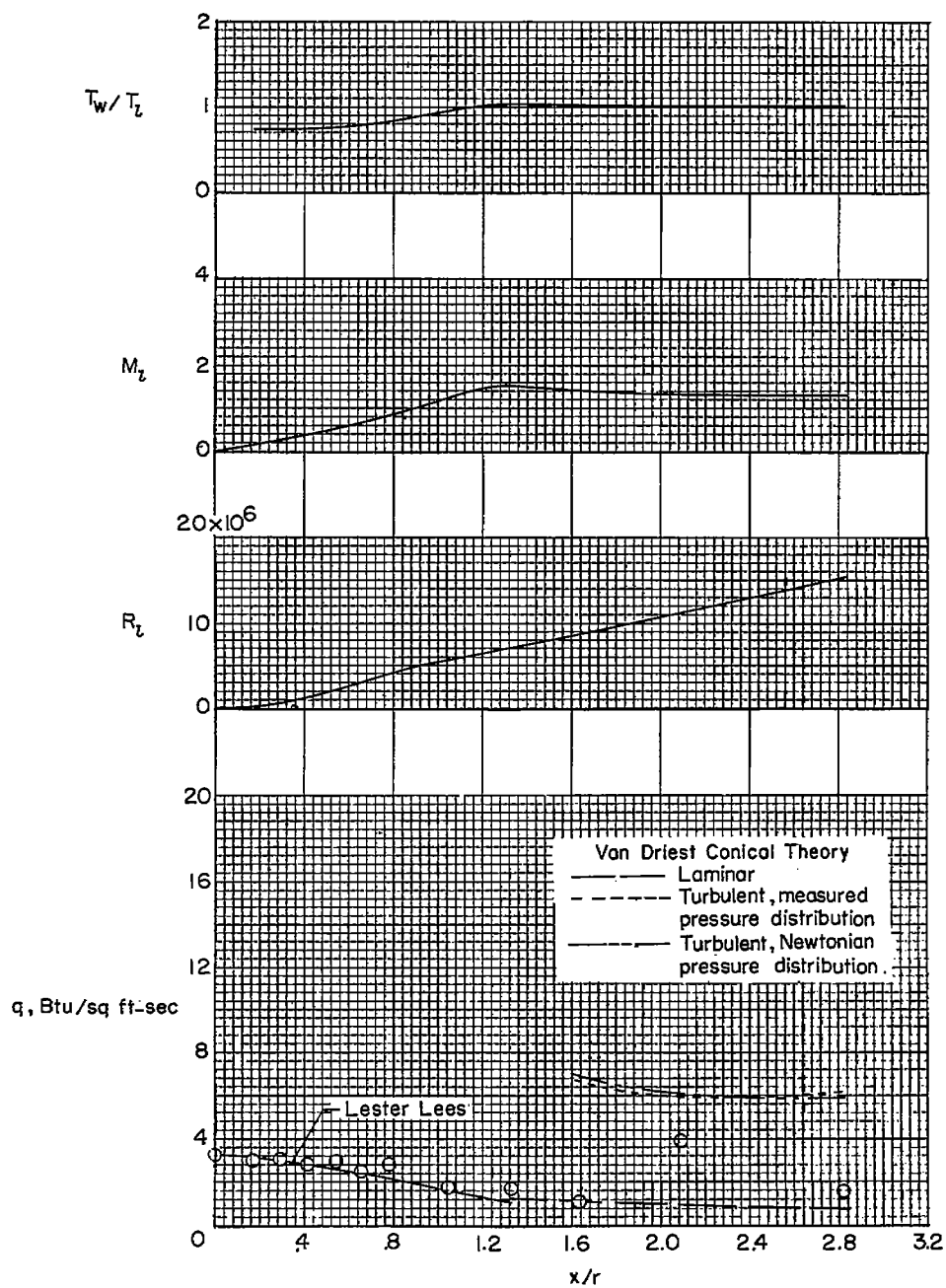
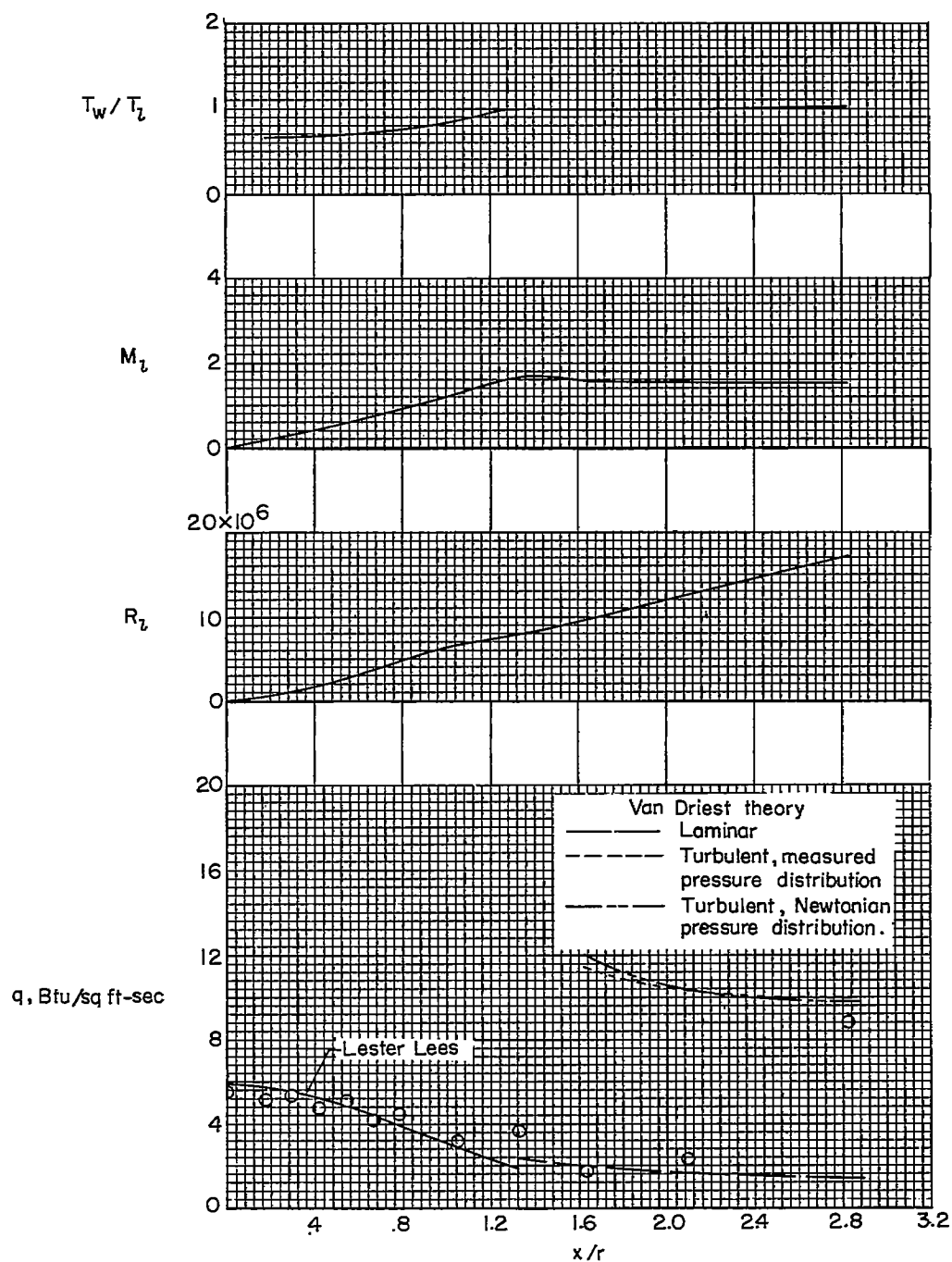


Figure 18.- Ratio of measured heating rate to measured heating rate at the stagnation point for the hemispherical portion of model B.



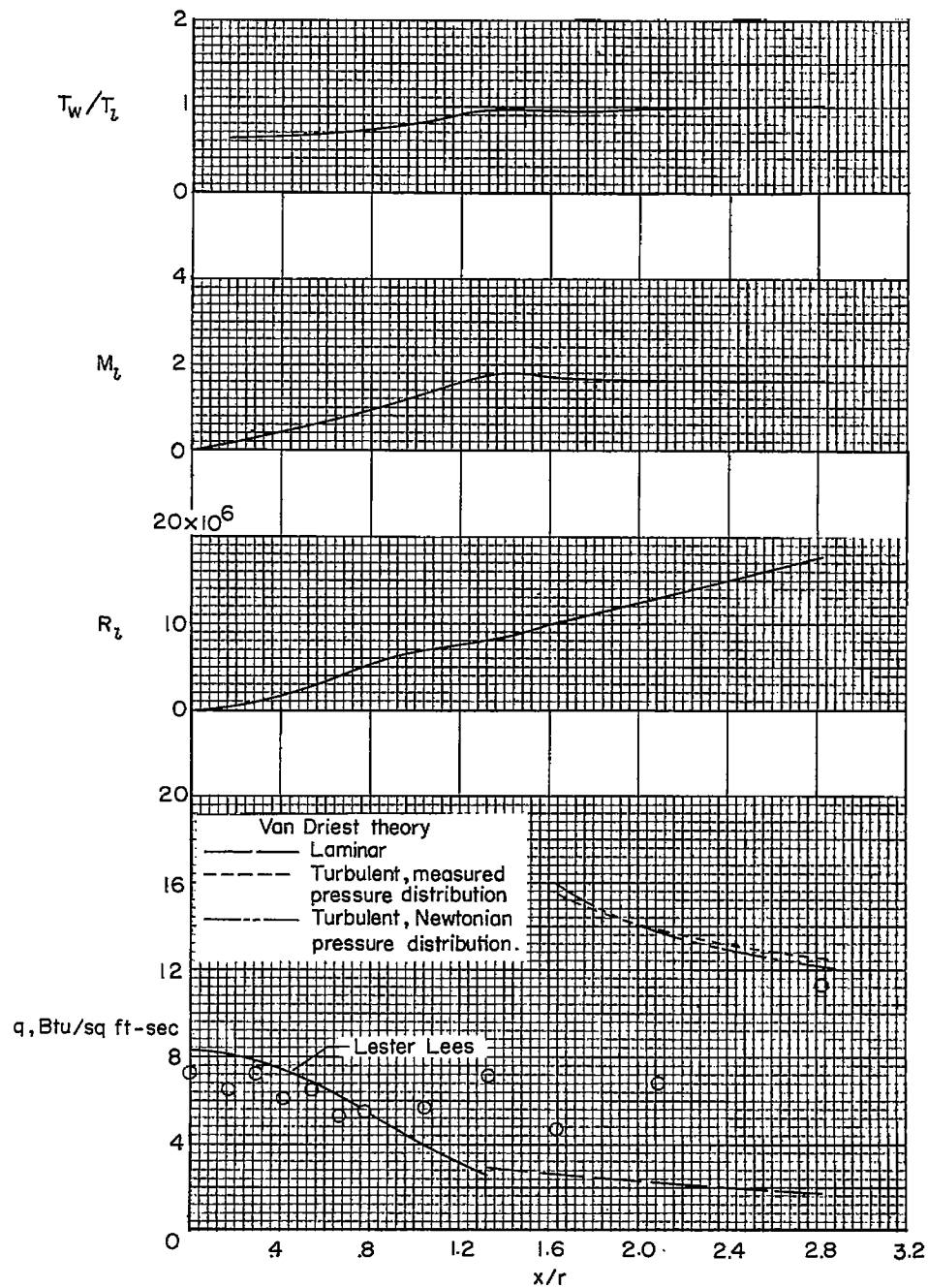
(a) $t = 3.2$ seconds; $M_\infty = 1.5$.

Figure 19.- Local heating rates, Reynolds number, and ratio of wall temperature to local static temperature for model B.



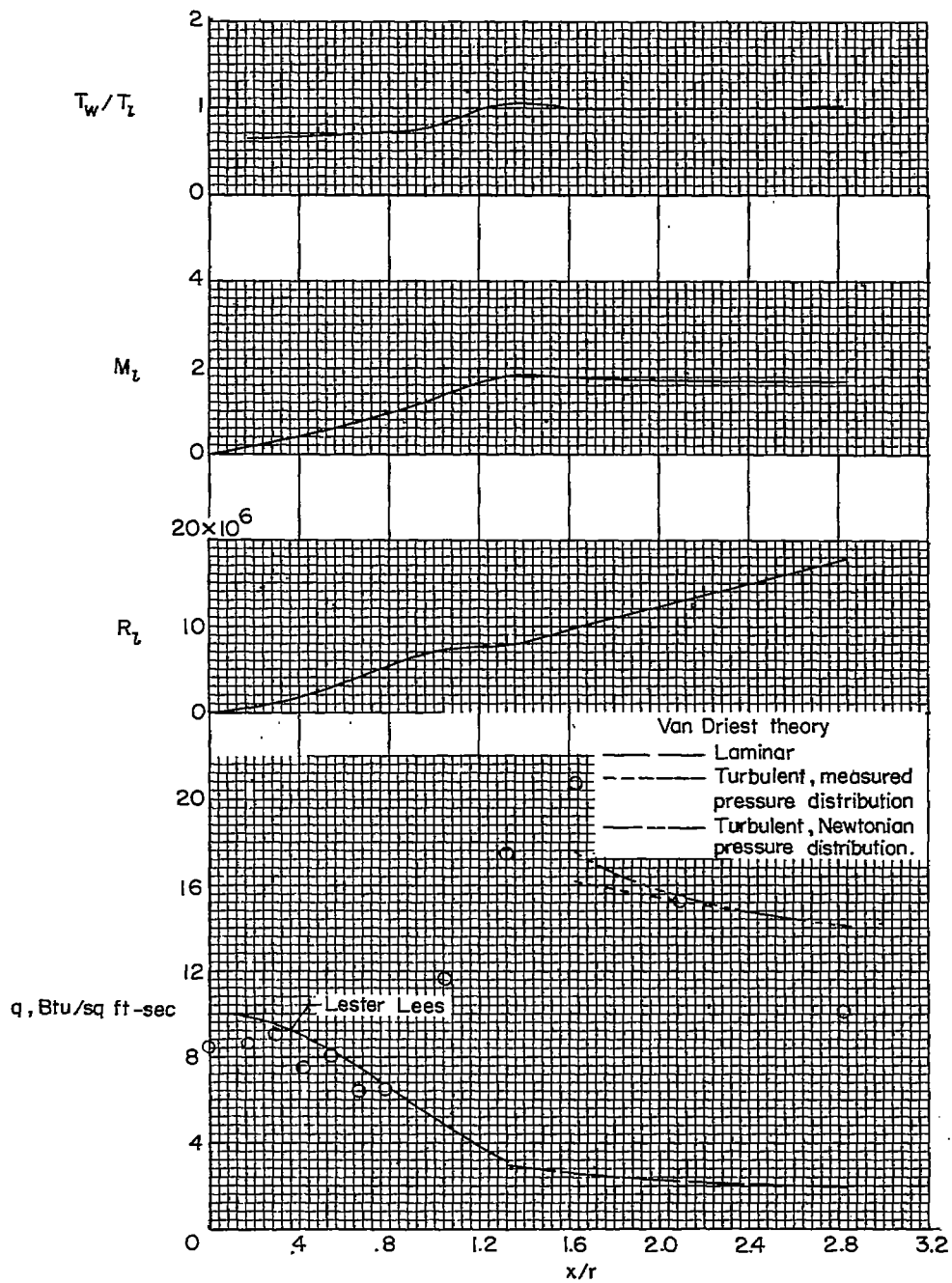
(b) $t = 3.8$ seconds; $M_\infty = 1.8$.

Figure 19.- Continued.



(c) $t = 4.2$ seconds; $M_\infty = 2.0$.

Figure 19.- Continued.



(d) $t = 4.7$ seconds; $M_\infty = 2.2$.

Figure 19.- Concluded.

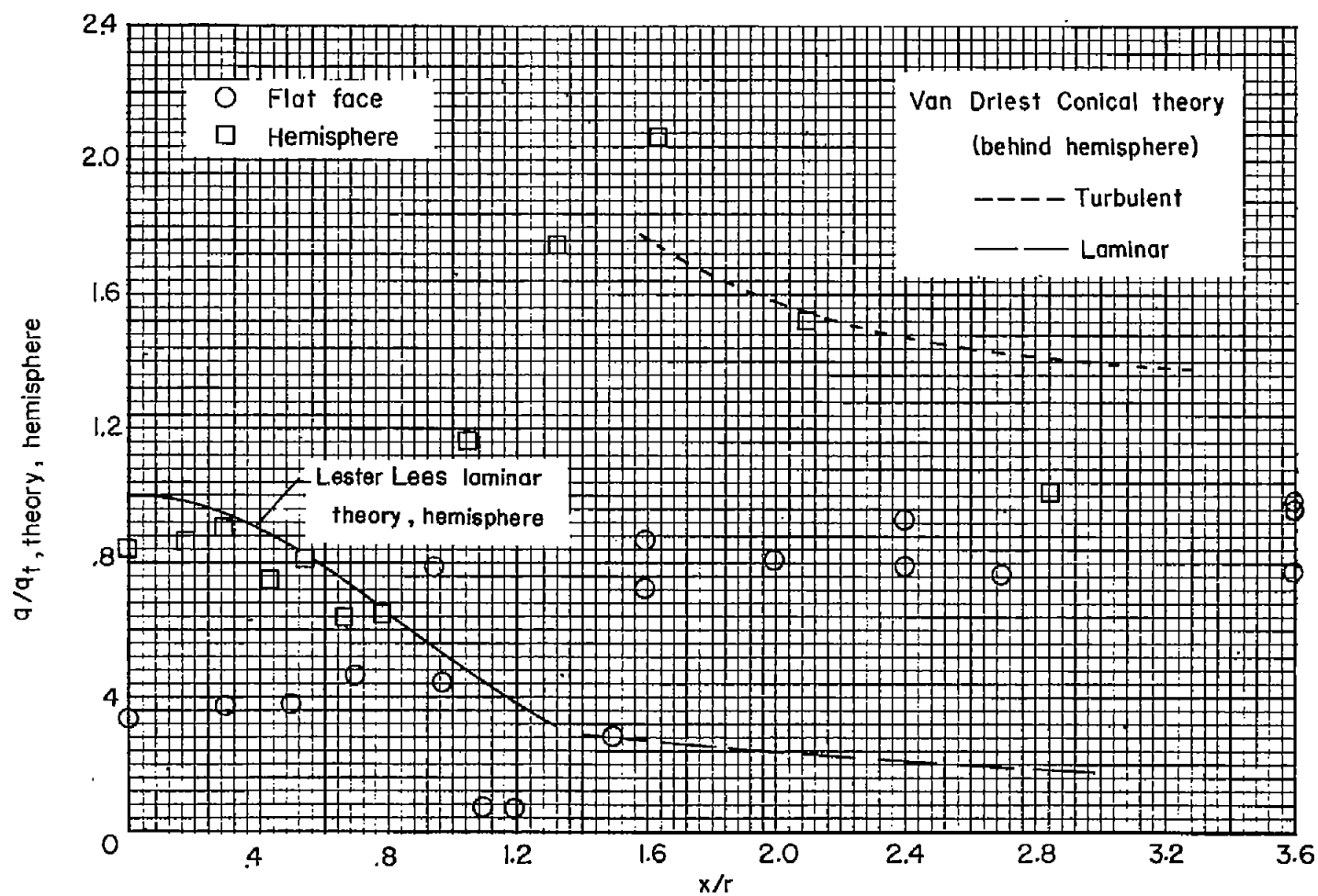


Figure 20.- Comparison of heating rates for the flat-face-cone and hemisphere-cone configurations. $M_\infty = 2.2$.